Nondirect transitions in variable-temperature angle-resolved photoemission from metals

R. C. White,* C. S. Fadley, and M. Sagurton†
Department of Chemistry, University of Hawaii at Manoa, Honolulu, Hawaii 96822

P. Roubin, D. Chandesris, J. Lecante, and C. Guillot
Service de Physique des Atomes et des Surfaces, Département de Physique Générale, Institut de Recherche Fondamentale de la Commissariat à l'Energie Atomique, Centre d'Etudes Nucléaires de Saclay, 91191 Gif-sur-Yvette Cédex, France

Z. Hussain
Department of Physics, University of Petroleum and Minerals, Dhahran 31261, Saudi Arabia
(Received 11 April 1986)

Temperature-dependent angle-resolved photoemission spectra have been obtained from Cu(001) for normal-emission conditions corresponding to direct transitions originating from various points along the $\Gamma-\Delta-X$ line. Photon energies were varied from 40 to 106 eV, and specimen temperatures were chosen between 77 and 977 K. Strong temperature dependence was observed at all photon energies, and this has been interpreted in terms of nondirect transitions localized about the expected direct transitions. Such phonon-assisted nondirect transitions are found to contribute significantly, even at low temperature. These nondirect transitions are also found to be semiquantitatively described by a simple modification of the direct-transition model incorporating cylindrical wave-vector broadening centered on the direct transition. Comparing experiment and theory permits estimating the degree of Brillouin-zone averaging involved at a given temperature. This modification of the direct-transition model is based on a more accurate theoretical treatment of such non-direct-transition effects. The consequences of such localized zone averaging due to nondirect transitions on earlier temperature-dependent data for Cu(110) and on studies of ferromagnetic metals near T_c are also discussed.

I. INTRODUCTION

Angle-resolved photoemission at energies $\lesssim 100$ eV is a very precise method for the determination of the electronic structure of solids.[1] However, the vast majority of previous measurements have been carried out at ambient temperature, with little or no temperature variation. Nonetheless, several prior studies have considered the temperature dependence of valence photoemission spectra from metals for a range of excitation energies from ultraviolet to x ray and from both experimental and theoretical points of view,[1-18] including considerations of the important ferromagnetic-to-paramagnetic transition.[14-18] Strong temperature effects on valence spectra were first observed experimentally by Williams *et al.*,[3] who reported a dramatic loss of intensity from an *s-p* band peak in Cu(011) with $h\nu=45$ eV as the specimen temperature was increased, and a rather quick convergence to spectra resembling the density of states. We will return to a discussion of the interpretation of this data later.

Several effects may occur as temperature is increased: Phonon-assisted nondirect transitions weaken the selection rule on $\mathbf{k}$, cause transitions from other regions of the Brillouin zone to be possible, and lead in a high-temperature limit to density-of-states-like spectra, in some way modulated by matrix elements. The lattice dilation with temperature, coupled with more complex electron-phonon interactions, may alter the initial- and final-state energies and wave functions,[2(c),5,10] and thus also change the matrix elements between them. Although several different theoretical approaches have been applied to describing one or more of these effects,[2,4-6,8-13,19] no fully quantitative model involving the full phonon spectrum and all orders of phonon processes has yet been applied to the analysis of experimental data. Initial-state shifts to lower binding energy due to lattice dilation are not expected to be larger than 0.1—0.2 eV, however, as the expected rates of change with temperature are only $(1-2)\times10^{-4}$ eV/K for Cu [Ref. 5(a)] and $(2-3)\times10^{-4}$ eV/K for Au [Ref. 5(b)].

In this study, we will focus on the disruption of $\mathbf{k}$ conservation during photoexcitation through phonon-assisted nondirect transitions (NDT's) which thus allow experimental sampling of points in $\mathbf{k}$ space not accessible in energy- and $\mathbf{k}$-conserving direct transitions (DT's). We will also focus primarily on photon energies $\gtrsim 30$ eV so that the final states can be reasonably well approximated as free-electron bands[20-23] for which a nonzero reciprocal-lattice vector is involved in the direct transitions, as illustrated in Fig. 1. Here, the initial wave vector $\mathbf{k}^i$ is taken to be in the reduced zone, whereas the final wave vector $\mathbf{k}^f$ is in the extended zone scheme. The first theoretical analysis focussing on these NDT effects was presented by Shevchik,[2(a)] who derived an expression for the thermally-averaged photocurrent based on a tight-binding initial state and a single plane-wave or augmented plane-wave final state. Although this analysis was subsequently extended,[2(b),2(c)] it is useful to quote Shevchik's simplest result for the temperature dependence of

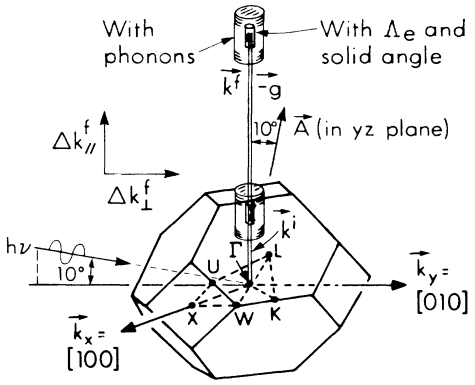

Direct: $\vec{k}^f = \vec{k}^i + \vec{g}$

$E^i(\vec{k}^i)$ = initial band structure

$E^f(\vec{k}^f) \approx \hbar^2 (k^f)^2/2m$

FIG. 1. The copper Brillouin zone, with normal-emission experimental geometry indicated. Also shown are the cylindrical **k** broadenings used to approximate effects due to the mean free path Λ_e ($\Delta k^f_{||}$), the analyzer acceptance solid angle ($\Delta k^f_{\perp}$), and phonon-assisted nondirect transitions (NDT's). These NDT's cause uncertainty in $\mathbf{k}^i$ for a given $\mathbf{k}^f$.

spectra.[2(a)] Here the photocurrent at finite temperature is written as a sum of a temperature-*independent* direct-transition component $I_{\rm DT}(E)$ and a temperature-*independent* non-direct-transition component $I_{\rm NDT}(E)$, modulated by factors depending upon the temperature-*dependent* bulk Debye-Waller factor $W(T)$:

$$I(E,T) = W(T) I_{\rm DT}(E) + [1 - W(T)] I_{\rm NDT}(E) , \qquad (1)$$

where $W(T) = \exp[-\frac{1}{3}\overline{U^2}(T) g^2]$ is the Debye-Waller factor, $\overline{U^2}(T)$ is the three-dimensional mean-squared vibrational displacement assuming uncorrelated atomic motion, and **g** is the reciprocal-lattice vector involved in the direct transitions. If additional phonon momentum is involved, then the relevant generalization on $W(T)$ can be obtained by replacing g^2 by $|\mathbf{k}^f - \mathbf{k}^i|^2 \equiv |\Delta\mathbf{k}|^2$. [Also, a more complex expression for $I(E,T)$ results if the full phonon spectrum is considered,[2(b),24] and we discuss this further below.] From Eq. (1), it follows that, as specimen temperature is increased, $W(T)$ decreases, and the nondirect contribution to the total photocurrent increases. Hence, $W(T)$ at this level of approximation provides an estimate of the fraction of transitions which are direct.

The temperature dependence suggested in Eq. (1) was first tested experimentally by Hussain *et al.* for angle-resolved x-ray photoemission (ARXPS) measurements on tungsten. They showed that pairs of spectra obtained at two different temperatures with angular resolutions of $\sim \pm 3°$ could be self-consistently deconvoluted to yield temperature-independent DT and NDT components. Furthermore, the positions of the major peaks in these DT components were found to be consistent with a straightforward DT model based on constant matrix elements and a final state satisfying the free-electron dispersion relation $E^f(k^f) = \hbar^2 (k^f)^2/2m$. The NDT components also closely resembled the density of states, as weighted by matrix elements appropriate to XPS. A more recent ARXPS study on tungsten with much higher angular resolutions of $\sim \pm 1.0°$ confirms these earlier conclusions, but also suggests that the DT components isolated via Eq. (1) may still contain significant NDT contributions.[25]

The same simple DT model has also been successfully used to describe ambient-temperature photoemission experiments on metals and semiconductors for $30 < h\nu < 140$ eV,[20–23] although no allowance has been made in these studies for the possible influence of nondirect transitions due to the much smaller **g** values involved as compared to the XPS case. Thus, questions arise as to how accurately initial-state energies can be determined for this energy regime in the presence of such NDT effects.

The analysis of temperature-dependent ultraviolet photoemission spectroscopy (UPS) data for Cu and Ag at $h\nu \leq 21.2$ eV by Mårtensson *et al.* has also indicated that most features which are presumed to be due to DT's empirically decay in intensity according to the functional form of the first term of Eq. (1).[9,11,12] However, the effective Debye-Waller factors thus derived are found to vary considerably from peak to peak and also with the emission geometry. Thus, the temperature dependence is found to depend strongly on the initial wave vector $\mathbf{k}^i$ being sampled. This has led to the proposal by Mårtensson[10] that vibrational lattice displacements may change the mixing coefficients in tight-binding states sufficiently to introduce an effective wave vector in the Debye-Waller factor that varies strongly with $\mathbf{k}^i$. No quantitative tests of this idea have been made, but it does qualitatively describe some aspects of the data. This model also implicitly neglects phonon-assisted nondirect-transition behavior.

A more complicated model for temperature-dependent valence spectra involving low-energy-electron-diffraction—type multiple-scattering calculations of thermally-averaged photoemission has been presented by Larsson and Pendry.[8] These calculations include vibrational effects via temperature-dependent scattering phase shifts and matrix elements, both of which are complex. Atomic vibrations are again assumed to be uncorrelated. Also, in order to make such calculations tractable, it was necessary to make approximations which result in the high-temperature photocurrent going to zero instead of the expected matrix-element-weighted density-of-states (DOS) limit. Thus, although the temperature dependence of sharp spectral features might be predicted by this model, background features expected to grow in at higher temperatures due to nondirect transitions distributed in some way throughout the Brillouin zone (BZ) are not expected to be described correctly. In fact, prior work shows that such time-reversed low-energy electron diffraction (LEED) calculations do not as yet fully predict the correct behavior of all of the sharp features observed in spectra.[8,9,11,12]

Temperature-dependent angle-resolved photoemission data have also been obtained by Jezequel *et al.*[13] for Pb(100) and Pb(110), where the low Debye temperature re-

quires cryogenic cooling to suppress nondirect transition effects. This work also suggests that enhanced surface vibrational amplitudes may be an important factor in determining the effective Debye-Waller factors involved. We will return to the latter point when discussing our results.

Prior studies involving either Eq. (1) or time-reversed LEED calculations have implicitly assumed that atomic vibrations are uncorrelated, so that a single mean-squared displacement is used to describe all atomic motion, regardless of the relative positions of any two atoms involved. Only proximity to the surface may be allowed for by using a larger mean-squared displacement.[8,11–13] The possible importance of correlated atomic motion among nearest neighbors on UPS spectra from more localized d-band states has been pointed out,[8] but no quantitative calculations including this effect have been carried out. Shevchik[2(b),2(c)] and, more recently, also Sagurton[24] have discussed the temperature dependence of one-electron matrix elements between tight-binding- or orthogonalized-plane-wave-like initial and final states, including to one degree or another the effects of correlated vibrations via summations over various phonon modes. Such one-electron matrix elements thus should involve a thermal average over all atomic displacements as produced by all combinations of thermally-excited phonon modes. All orders of phonon absorption and/or emission during photoexcitation are included in the more accurate Sagurton result, which we discuss in more detail below. Both of these analyses give rise to the following general conclusions however.

(1) The temperature dependence of DT intensity is still described by a Debye-Waller factor.

(2) The temperature dependence of NDT intensity is more complex than Eq. (1), with both a Debye-Waller prefactor and a complex summation over various thermally-excited phonon modes. Thus, the expression for the photocurrent is modified to

$$I(E,T)=W(T)I^{*}_{\mathrm{DT}}(E)+I^{*}_{\mathrm{NDT}}(E,T)\ , \tag{2}$$

where I^{*}_{DT} and I^{*}_{NDT} are the true direct- and non-direct-transition currents as predicted by theory. Thus, a clean separation of DT and NDT components via temperature-dependent data and Eq. (1) is called into question, as confirmed in a recent ARXPS study of W.[25]

(3) The phonon-assisted nondirect transitions of highest probability are those of shortest total phonon wave vector $\mathbf{Q}$. Thus, the NDT intensity associated with emission from a given initial wave vector $\mathbf{k}^i$ in the reduced zone will tend to be localized around $\mathbf{k}^i$. Stated in another way, nondirect transitions will tend to be peaked around direct transitions, a result completely analogous to the peaking of thermal diffuse scattering around Bragg peaks in x-ray diffraction[26] or low-energy electron diffraction.[27] This last conclusion is thus suggestive in connection with the previously-mentioned results for Cu,[3,5(a),8,9,11] Ag,[12] and Pb,[13] as well as for ferromagnetic Fe(001) with $h\nu=20$–70 eV,[18] in which it is found that the temperature-induced changes in different features are strongly dependent on $\mathbf{k}^i$. Thus, the NDT aspect of these temperature dependences may be more important than previously realized, a point we discuss in detail here.

In this study, we present an extensive set of temperature-dependent UPS data from Cu(001) obtained using synchrotron radiation in the range 40–106 eV. The very strong temperature effects observed in these results are interpreted in terms of nondirect transitions localized about the expected direct transitions. A more accurate theoretical treatment of such NDT effects due to Sagurton[24] is discussed. The localized NDT's are calculated within the simple DT model by including a cylindrical averaging in $\mathbf{k}^i$ with variable volume. Additional zone-averaging effects due to the analyzer angular acceptance and electron inelastic scattering are also included. The effects of such localized zone averaging due to nondirect transitions on prior experimental data for Cu(110) (Ref. 3) and on studies of ferromagnetic metals near T_c are also discussed. A preliminary account of this work will appear elsewhere.[28]

II. EXPERIMENTAL PROCEDURE

Angle-resolved valence photoemission spectra were obtained using radiation from the 540 MeV ACO (les Anneaux de Collisions) storage ring at Laboratoire pour l'Utilisation du Rayonnement Electromagnétique (LURE) in Orsay. The excitation energy was varied from 40 to 106 eV using a high-flux toroidal grating monochromator. Normal emission from Cu(001) was employed, allowing the sampling of initial states along the Γ–Δ–X direction. The energy resolution for the combined monochromator/analyzer system varied from $\sim$130 meV at low photon energies to $\sim$170 meV at high energies. The chamber and experimental equipment have been described elsewhere.[23] The experimental geometry for this series of experiments is shown in Fig. 1, as is the reduced Brillouin zone of copper. The photon flux was incident on a clean Cu(001) specimen at an angle of 80° with respect to the surface normal and in the yz plane of mirror symmetry. This experimental geometry results in almost completely p-polarized radiation, since $\mathbf{A}$ is only 10° off the surface normal. Thiry[23(b)] has studied ambient-temperature normal emission from Cu(001) in the same geometry, and wherever comparisons are possible, our results agree fully with his.

From the symmetry-based selection rules for this geometry,[23(b),29] emission from bands of Δ_1 symmetry is preferentially selected, with emission from bands of Δ_2 and Δ_2' being forbidden and that from bands of Δ_5 symmetry being substantially weaker due to an almost forbidden geometry. Figure 2 presents the Cu band structure of Burdick,[30] with the bands coded according to the symmetry selection rules mentioned above. Also indicated here are the simple direct transitions sampled for three of the photon energies studied: 40.8, 66.1, and 97.3 eV. These energies are chosen to yield $\mathbf{k}^i$ points via simple direct transitions to free-electron final states that are centered at Γ [$\mathbf{k}^i=(0,0,0)2\pi/a$], midway along Δ [$\mathbf{k}^i=(0,0,\frac{1}{2})2\pi/a$], and at X [$\mathbf{k}^i=(0,0,1)2\pi/a$], respectively, a procedure used in prior studies of this system.[20,23] Further energies studied and their corresponding $\mathbf{k}^i$ points were as follows: 52.7 eV [$\mathbf{k}^i=(0,0,\frac{1}{4})2\pi/a$], 81.0 eV [$\mathbf{k}^i=(0,0,\frac{3}{4})2\pi/a$], 89.0 eV [$\mathbf{k}^i=(0,0,\frac{7}{8})2\pi/a$], and

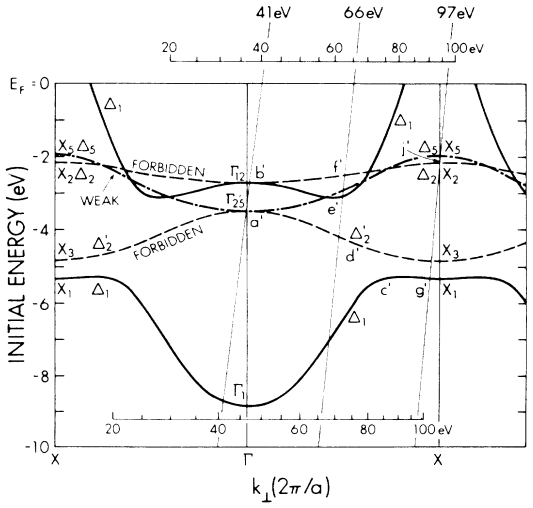

FIG. 2. The copper band structure of Burdick (Ref. 30) along $\Gamma-\Delta-X$ is shown together with the $\mathbf{k}^i$ points sampled by simple direct transitions at $h\nu=41$, 66, and 97 eV. Features in the theoretical spectra that are of simple origin are indicated as a', b', c', . . . , and in most cases correlate directly with features a, b, c, . . . in experimental spectra, respectively.

105.9 eV [$\mathbf{k}^i=(0,0,-\frac{7}{8})2\pi/a$]. The direct transitions for $h\nu=40.8-97.3$ eV involve $\mathbf{g}=(0,0,2)2\pi/a$, while those for $h\nu=105.9$ eV are formally equivalent to those for $h\nu=89.0$ eV except that the former involve $\mathbf{g}=(0,0,4)2\pi/a$. This difference between 89.0 and 105.9 eV thus may permit the observation of photoemission from the same BZ points but with different thermal properties owing to the dependence of the effective Debye-Waller factor $W(T)$ on the $\mathbf{g}$ involved in the transition.

Specimen temperature was varied from 77 to 977 K, the widest range to date for experiments of this kind. A liquid-nitrogen cold finger was attached directly to the specimen in attaining the lowest temperature. Higher temperatures were measured with a thermocouple-calibrated infrared pyrometer.

The angular resolution of the lens-analyzer system utilized is estimated to be $\sim\pm0.5°$.[23] This high resolution, along with the low-temperature capability, thus provides the best possible opportunity for the observation of direct transitions with minimum additional broadening in $\mathbf{k}$. Inelastic backgrounds were subtracted from some of the data presented here using an iterative, self-consistent procedure described elsewhere.[6,31]

The necessity to step temperatures and then wait for full thermal equilibrium, coupled with time-dependent drifts in the storage ring current and periodic mirror and monochromator adjustments, prevented obtainment of reliable comparisons of absolute spectral intensities from one temperature to another, although recent ARXPS data of this kind are discussed elsewhere.[25] Thus, we will confine our discussion here to the positions and relative intensities of different features in spectra as a function of temperature.

III. RESULTS AND DISCUSSION

A. Qualitative features of Cu(001) temperature dependence

In Figs. 3 through 5, we show valence spectra taken at specimen temperatures of 77 K and room temperature for six photon energies corresponding to direct transitions from various points along the Γ to X line, all with the same mediating $\mathbf{g}$ of $(0,0,2)2\pi/a$. Also given in these figures are the bulk Debye-Waller factors (W), calculated for

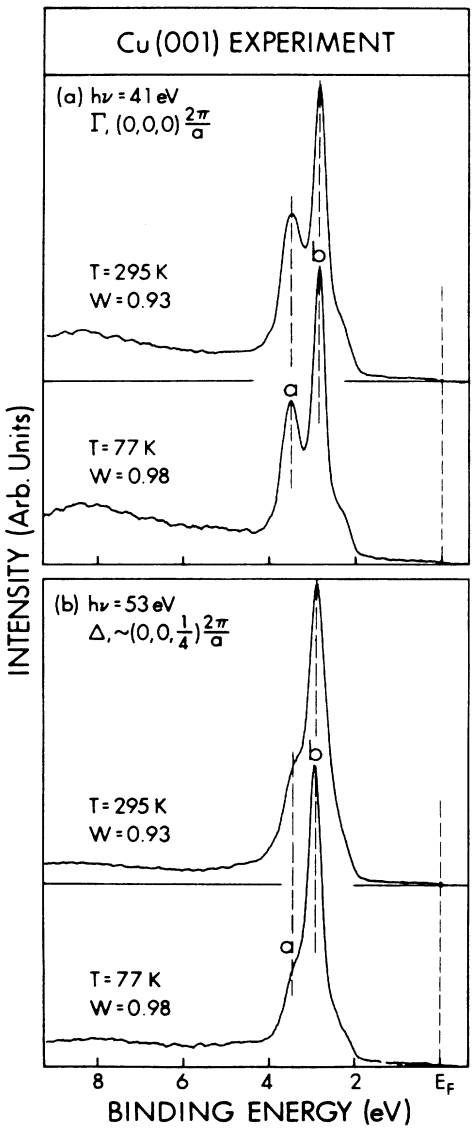

FIG. 3. Normal-emission valence spectra for Cu(001) taken at specimen temperatures of 77 and 295 K for (a) $h\nu=41$ eV, corresponding to simple direct transitions from the Γ point, and (b) $h\nu=53$ eV, corresponding to direct transitions from a Δ point $\frac{1}{4}$ of the distance from Γ to X. Also given are the bulk Debye-Waller factors W at the two specimen temperatures. Features a and b can be related to emission from Γ_{25}' and Γ_{12}, respectively (cf. a' and b' in Fig. 2).

a Debye temperature (Θ_D) of 343 K. Although, as discussed previously, enhanced surface vibrations may lead to effectively lower W values, these bulk values nonetheless provide a rough estimate of the degree of nondirect transitions expected via $1-W$ in the simple model of Eq. (1). This point will be discussed further in Secs. III B and III C. The low-temperature spectra, where one thus expects ~98% direct transitions can be compared directly with the band structure in Fig. 2 in order to determine major peak origins. This procedure has been used with similar ambient-temperature spectra by Thiry.[23(b)]

In Fig. 3, spectra for $h\nu=41$ and 53 eV are shown. For 41 eV, features a and b can be traced in origin to a' (Γ'_{25}) and b' (Γ_{12}) in Fig. 2. The low relative intensity of a is expected, since it arises from a weakly contributing Δ_5 band, while b is primarily of allowed Δ_1 origin. Although the 41 eV peak positions remain constant on increasing specimen temperature to 295 K, there is a significant broadening and filling in of the valley between a and b. For $h\nu=53$ eV and $T=77$ K, the main peak directly re-

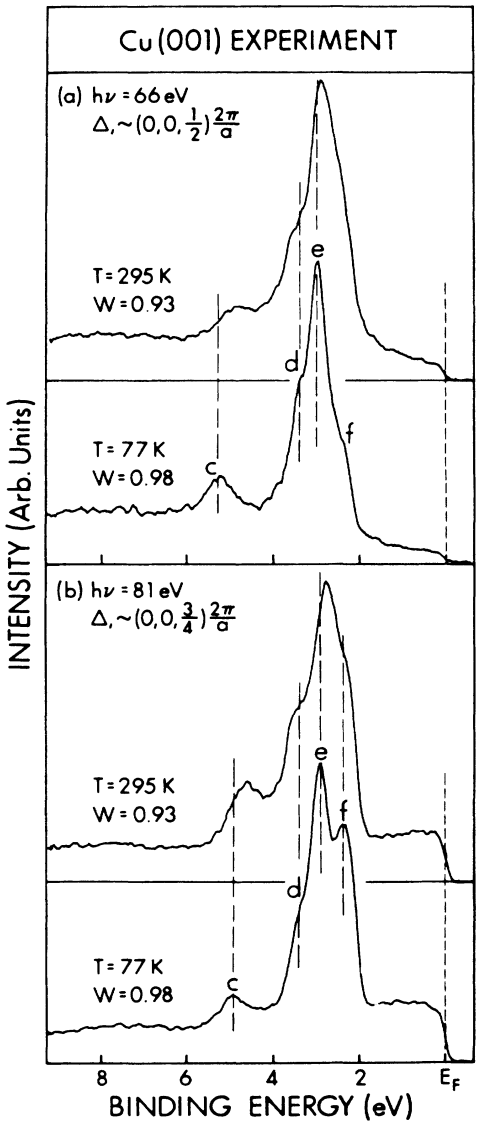

FIG. 4. As Fig. 3, but for (a) $h\nu=66$ eV corresponding to direct transitions from a Δ point halfway between Γ and X, and (b) $h\nu=81$ eV corresponding to direct transitions from a Δ point at $\frac{3}{4}$ of the distance from Γ to X. Features c and f can be related to specific bands if broadening effects are included, but d and e largely involve an umklapp process from the Γ point. Note the significant shift of feature c and to a lesser degree also d on going from 77 to 295 K.

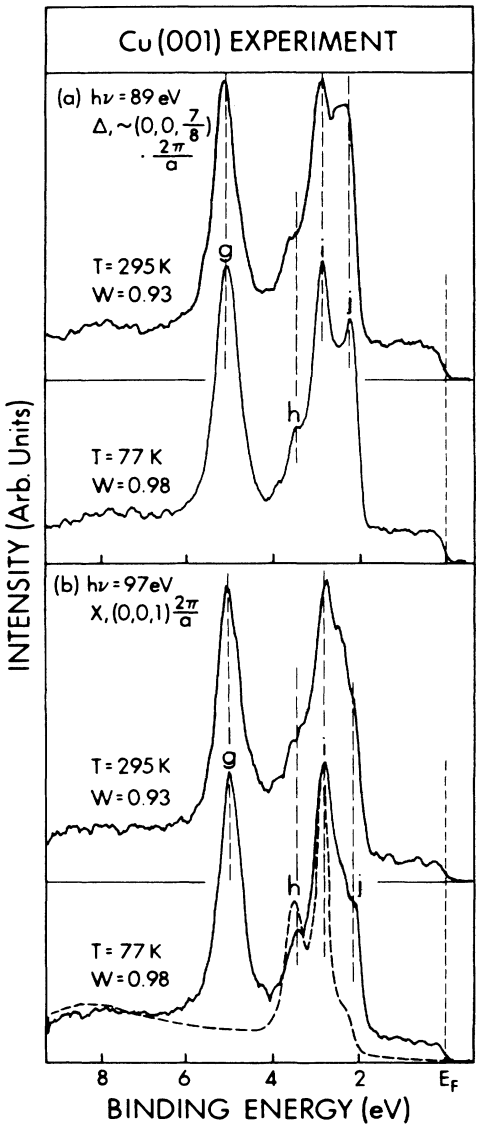

FIG. 5. As Fig. 3, but for (a) $h\nu=89$ eV corresponding to direct-transition emission from a point $\frac{7}{8}$ of the distance from Γ to X, and (b) $h\nu=97$ eV corresponding to emission from the X point. The dashed curve in (b) is the Γ spectrum at 77 K from Fig. 3(a), and it indicates that much of the intensity of features h and i here (or of d and e in Fig. 4) arise from a surface umklapp process.

lated to b' shifts to slightly higher binding energy by ~ 0.1 eV as compared to the analogous 41 eV peak, thus following the dispersion of the Δ_1 band. Also, the closing of the Δ_1-Δ_2 gap due to dispersion suppresses the a/b splitting and places the shoulder related to peak a at lower binding energy. For this case, more than for 41 eV, there is an overall broadening as temperature is increased to 295 K, with this being due to a greater enhancement of the relative intensities of both the a-related feature at 3.5 eV and in the region from ~ 2.0—2.7 eV. The position of the main b peak does not change with temperature, however, in agreement with its behavior at 41 eV.

For points further along the Δ line at $h\nu = 66$ and 81 eV, as shown in Fig. 4, the situation is more complicated. Considering first the 77 K results that should be most simply related to direct transitions, we see that the strongest peak e (related to peak b in Fig. 3 in origin) exhibits a slow shift toward E_F as $h\nu$ increases. This shift is qualitatively consistent with the upward dispersion of the Δ_1 band in this photon energy region, but is much smaller than expected from the calculated band structure (cf. Fig. 2). An additional feature c at ~ 4.9—5.2 eV is also seen in these spectra, with its position and sharpness suggesting that it is due to some residual $\mathbf{k}$ smearing that allows transitions from the flatter portion of the lowest Δ_1 band near X, as labeled c' in Fig. 2. The possible simple DT origins of peaks d and f are indicated as d' and f' in Fig. 2, although the Δ_2 and Δ_2' bands involved are nominally forbidden. An additional explanation for peaks d and e in terms of a surface umklapp process[23(b)] is discussed below. Also, $\mathbf{k}^i$ broadening around the relevant Δ point is probably sufficient to allow transitions in feature f to arise from the partially allowed Δ_5 band near j'. There is also a striking increase in the relative intensity of the s-p band contribution between 0.0 and 1.8 eV as $h\nu$ changes from 66 to 81 eV. This also is consistent with the DT's expected in Fig. 2. As temperature is increased to ambient for both energies, major changes in both peak positions and relative intensities are seen. For example, as T is increased, peak c shifts to lower binding energy by 0.4—0.5 eV in both cases, the relative intensity in the region of f increases significantly, the resolution of e and f is reduced at 81 eV, and shoulder d increases in relative intensity and shifts to higher binding energy by ~ 0.2 eV in both cases. Thus, it is clear for these two photon energies corresponding to Δ points with relatively high band dispersions that thermal effects over even this narrow temperature range from 77 to 295 K can easily cause shifts of a few tenths of an eV *and* very significant changes in spectral shapes and relative intensities. This range furthermore represents only a 0.05 change in the bulk Debye-Waller factor, or equivalently an estimated 5% increase in the total percentage of nondirect transitions. Initial-state energy shifts alone are also quite inadequate to explain the peak shifts observed, particularly that of peak c. From a prior analysis of Cu(001) photoemission,[5(a)] only an approximately 0.2 eV shift to *lower binding energy* is expected over this 218 K temperature range. This data thus by itself calls into question the accuracy with which ambient-temperature spectra can be used to experimentally determine band structures.

The spectra for photon energies of 89 and 97 eV are shown in Fig. 5. Those at 77 K exhibit a dramatic increase in peak g (which is related to c in Fig. 4) associated with the flat Δ_1 band near g' in Fig. 2. The relative intensities of features h, i, and j (related to d, e, and f in Fig. 4) also change over these two energies, with a much more pronounced i-j separation at 89 eV. Figure 2, however, suggests that only features g and j, due respectively to an allowed Δ_1 band (near g') and a partially allowed Δ_5 band (near j'), should be observed experimentally. Thiry[23(b)] has interpreted features h and i as being due to an umklapp process involving Γ-point emission and surface $\mathbf{g}$ vectors of the type $(0,2,0)2\pi/a$. This umklapp involves flat bands near Γ over the energy range $70 \lesssim h\nu \lesssim 100$ eV,[23(b)] and is this expected to be most evident for these energies. In Mahan's nomenclature,[32] it corresponds to a secondary cone in Γ emission at these photon energies that is oriented at angles of $\sim 40°$—$50°$ with respect to the primary non-normal emission. The dashed curve in Fig. 5(b) shows the Γ spectrum at 77 K of Fig. 3(a), and this umklapp interpretation is seen to be very reasonable in terms of the positions of both h and i and to a lesser degree of their relative intensities. The low-temperature data make this analysis in terms of an umklapp event much clearer then in previous work, however. This conclusion also suggests that some, if not most, of the intensity of features d and e in Fig. 4 is associated with this Γ umklapp. In fact, $h\nu = 81$ eV should correspond to emission centered closest to Γ,[23(b)] and it is here that the d/e relative intensity is also closest to the a/b relative intensity in Fig. 3.

The changes in the spectra in Fig. 5 with temperature are less dramatic than those in Fig. 4, but small shifts (e.g., of g and h) as well as significant relative intensity changes (e.g., of i and j) are seen. This lower sensitivity is consistent with the fact that the initial states involved here at X or, via the umklapp, near Γ, are also very low in dispersion. Figure 5 also provides evidence for some residual degree of zone averaging in the 77 K spectra for 89 eV and, to a lesser degree, for 97 eV, because the s-p band intensity from 0.0 to 1.8 eV is quite strong (especially at 89 eV) even though Fig. 2 indicates it should not be present. We will discuss the modeling of such zone averaging in terms of contributions due to inelastic scattering, the analyzer angular acceptance, and phonon-assisted NDT's in the following sections.

In Fig. 6, we show room-temperature spectra for $h\nu = 89$ eV and $h\nu = 106$ eV, along with the relevant W values and the $\mathbf{g}$ vectors mediating the direct transitions. These two spectra are therefore, in principle, sampling the same BZ point, but there is a strong indication of enhanced thermal effects for 106 eV with the larger $\mathbf{g}$ vector as a significant filling in of the valley between features g and i-j and a loss of resolution of features i and j that cannot be fully explained in terms of the decreased instrumental resolution as energy is increased.

In Figs. 7, 8, and 9, we consider temperature dependence over a much broader range from 77 to 977 K for three photon energies of 41, 81, and 97 eV, respectively. Here the inelastic background previously present in Figs. 3—6 has been subtracted in a self-consistent way[6,31] to

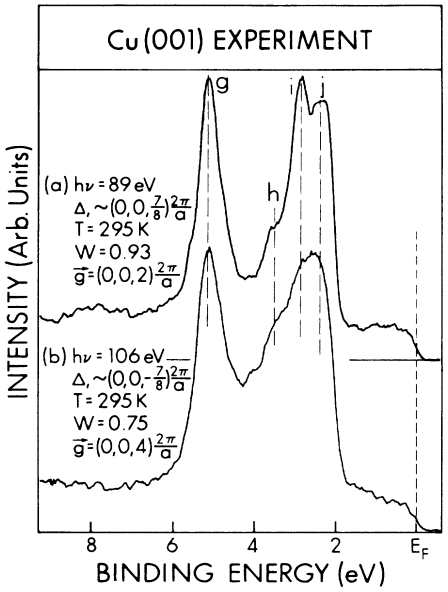

FIG. 6. Normal-emission valence spectra for Cu(001) taken at 295 K and with photon energies of (a) 89 eV and (b) 106 eV corresponding to direct-transition emission from two symmetry-equivalent Δ points near X in the BZ. Also given are the bulk Debye-Waller factors and the **g** vectors involved. The major difference between the two spectra thus should be the mediating **g** vector for the direct transitions.

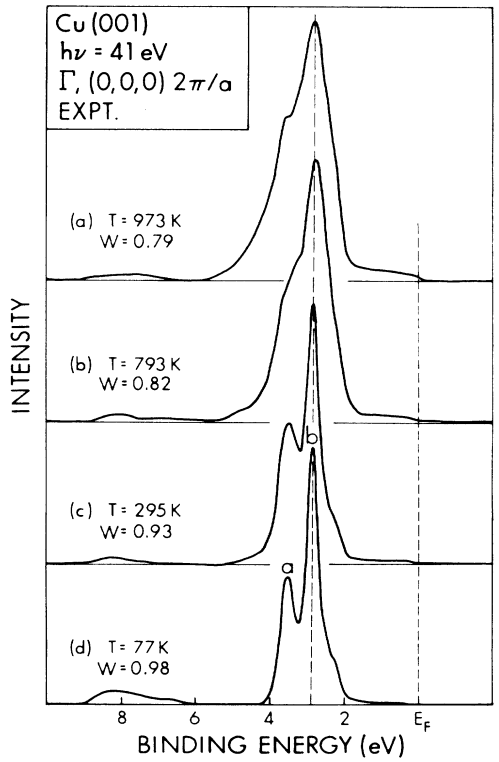

FIG. 7. Temperature-dependent spectra for normal emission from Cu(001) at $h\nu=41$ eV. Temperatures between 77 and 973 K are shown.

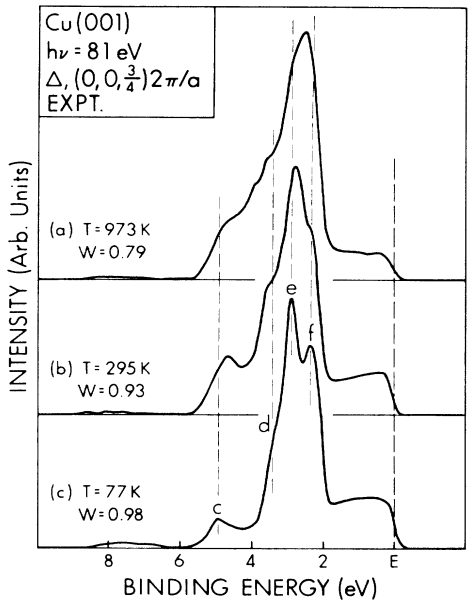

FIG. 8. Same as Fig. 7, but for $h\nu=81$ eV and Δ-point emission.

permit easier identification of fine structure and more direct comparison to DT calculations. For $h\nu=41$ eV in Fig. 7, the valley between a and b is completely filled in by 793 K, even though the difference in the Debye-Waller factors between 295 and 793 K is only 0.11. At $T=973$ K with $W=0.79$, the spectrum is further broadened slightly, but it is noteworthy that it still retains the gross shape of the low T spectra; thus, although the overall a-b

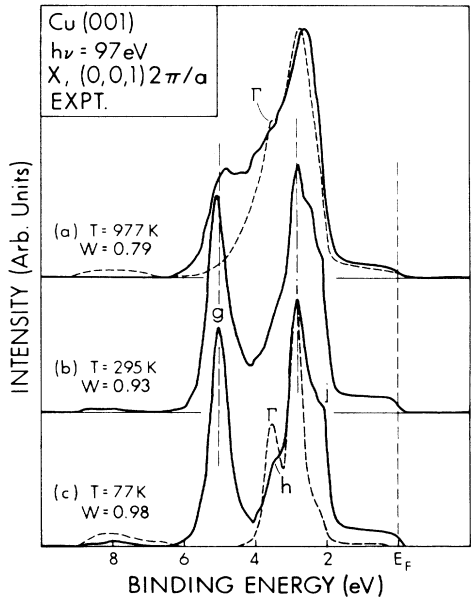

FIG. 9. Same as Fig. 7, but for $h\nu=97$ eV and X-point emission. In (a) and (c) we also show corresponding Γ-point spectra from Fig. 7 that may be involved due to an umklapp process.

width has increased from a full width at half maximum (FWHM) of 0.96 eV to 1.50 eV, the DOS limit has clearly not been reached. This behavior can be contrasted with prior studies involving much lower Debye-Waller factors in which a DOS limit does appear to be reached: XPS measurements on tungsten with $W=0.14$ (Refs. 6 and 25) and UPS measurements on lead with $W\approx 0.26$ (Ref. 13).

For $h\nu=81$ eV in Fig. 8, features *e* and *f* are clearly resolved only at 77 K, and there is a significant shift of the resultant featureless spectral maximum to lower binding energy by ~ 0.4 eV as temperature is raised to 973 K. There is also a rather complete filling in of intensity between features *c* and *d* at the highest temperature. Finally, the *s-p* band intensity for 0—1.8 eV decreases significantly in relative intensity as temperature is increased. However, the general shape of the 973 K spectrum is still very similar to that at 77 K, indicating once again that a DOS limit has not been reached.

For $h\nu=97$ eV in Fig. 9, the valley between *g* and *i* is completely filled in as temperature is increased to 977 K, although a small shifted peak near *g* is still apparent and the principal peak near *i* remains. There is a complete loss of shoulders *h* and *j* on going to high temperature. We have included in Figs. 9(a) and 9(c) the Γ-point spectra at corresponding temperatures as dashed curves to indicate possible intensity due to the previously discussed umklapp process. It is thus possible that a significant fraction of the dominant high-temperature peak centered at the position of peak *i* is due to such Γ-point emission, as broadened by thermal effects.

B. Theoretical model including the effects of correlated vibrations

The thermal effects on spectra in Figs. 3—9 are thus considerable, and, before trying to interpret them more quantitatively, we here briefly consider a recent theoretical model due to Sagurton[24] that emphasizes phonon-assisted nondirect transitions as produced by correlated atomic motion. Thus, we will neglect any effects due to changes in the initial-state energies or hybridization of wave functions and concentrate on only those aspects of thermal motion which disturb **k** conservation in photoexcitation. Although it certainly may ultimately be necessary to include these additional effects, this approach has the advantage of finally permitting a relatively simple estimate of NDT contributions to spectra via the simple direct-transition model of Ref. 6. This analysis thus goes beyond the prior work of Shevchik[2(b),2(c)] and Sayers and McFeely[4] in several respects as far as the inclusion of phonon effects is concerned, although in stressing the relaxation of **k** conservation it focuses on what are termed "intra-atomic" electron-phonon interactions in the Shevchik terminology.[2(c)]

Prior general theoretical treatments of angle-resolved photoemission[32,33] neglect thermal motion and adopt the classical viewpoint that atoms occupy definite lattice positions at time *t*, with the total photocurrent in the direction of the detector $\mathbf{k}^f$ finally given as

$$I(\mathbf{k}^f, E=E^f)\propto v\sum_i \delta(E^f-E^{i(0)}-\hbar\omega)\times\left|\int d^3r\,\psi^{f(0)*}_{\mathbf{k}^f}(\mathbf{r})\mathbf{A}(\mathbf{r})\cdot\mathbf{p}\psi^{i(0)}_{\mathbf{k}^i}(\mathbf{r})\right|^2$$
$$\propto v\sum_i \delta(E^f-E^{i(0)}-\hbar\omega)\,|M^{(0)}_{if}|^2\,, \tag{3}$$

where v is the photoelectron velocity in vacuum, the δ function ensures energy conservation, the superscripts $f(i)$ denote final- (initial-) state values, and the superscript (0) denotes quantities evaluated for the rigid equilibrium lattice. Since the photoemission process, in general, occurs on a shorter time scale than that of a typical lattice vibration, Eq. (3) thus can also be used to describe the photocurrent at time t for a vibrating lattice if the energies and wave functions of the equilibrium lattice are replaced by their corresponding values computed for the displaced lattice at time t. The thermally-averaged photocurrent is then obtained by summing or integrating Eq. (3) over all lattice displacements with appropriate statistical weightings.

During photoexcitation, the displacement $\mathbf{U}_l$ of the lth atom from its equilibrium position $\mathbf{R}^{(0)}_l$ is given in terms of the bulk normal modes of the solid as

$$\mathbf{U}_l=\mathbf{R}_l-\mathbf{R}^{(0)}_l=\sum_{\mathbf{q},\hat{\boldsymbol{\epsilon}}}\mathbf{U}_{l,\mathbf{q},\hat{\boldsymbol{\epsilon}}} \tag{4a}$$
$$=\tfrac{1}{2}\sum_{\mathbf{q},\hat{\boldsymbol{\epsilon}}}A_{\mathbf{q},\hat{\boldsymbol{\epsilon}}}\hat{\boldsymbol{\epsilon}}\{\exp[i(\mathbf{q}\cdot\mathbf{R}^{(0)}_l+\delta_{\mathbf{q},\hat{\boldsymbol{\epsilon}}})]+\exp[-i(\mathbf{q}\cdot\mathbf{R}^{(0)}_l+\delta_{\mathbf{q},\hat{\boldsymbol{\epsilon}}})]\}\,, \tag{4b}$$

where $A_{\mathbf{q},\hat{\boldsymbol{\epsilon}}}$ is the amplitude of the oscillation of a given phonon mode with wave vector $\mathbf{q}$ and polarization $\hat{\boldsymbol{\epsilon}}$, and $\delta_{\mathbf{q},\hat{\boldsymbol{\epsilon}}}$ is the phase. The phonon amplitude is given in the harmonic approximation by

$$A^2_{\mathbf{q},\hat{\boldsymbol{\epsilon}}}=\frac{2\hbar}{MN\omega_{\mathbf{q},\hat{\boldsymbol{\epsilon}}}}(n_{\mathbf{q},\hat{\boldsymbol{\epsilon}}}+\tfrac{1}{2})\,, \tag{5}$$

where $n_{\mathbf{q},\hat{\boldsymbol{\epsilon}}}$ is the occupation number of mode $\mathbf{q},\hat{\boldsymbol{\epsilon}}$, M is the atomic mass, N is the number of atoms, $\omega_{\mathbf{q},\hat{\boldsymbol{\epsilon}}}$ is the frequency, and the energy associated with this mode is $\hbar\omega_{\mathbf{q},\hat{\boldsymbol{\epsilon}}}(n_{\mathbf{q},\hat{\boldsymbol{\epsilon}}}+\frac{1}{2})$.

It is now assumed that the set of phonon phases $\{\delta_{\mathbf{q},\hat{\boldsymbol{\epsilon}}}\}$ associated with a given set of occupation numbers $\{n_{\mathbf{q},\hat{\boldsymbol{\epsilon}}}\}$ can be averaged over to yield a phase-averaged photocurrent

$$I(\mathbf{k}^f,E,\{n_{\mathbf{q},\hat{\boldsymbol{\epsilon}}}\})=\langle I(\mathbf{k}^f,E,\{n_{\mathbf{q},\hat{\boldsymbol{\epsilon}}},\delta_{\mathbf{q},\hat{\boldsymbol{\epsilon}}}\})\rangle_{\text{phase}}\,, \tag{6}$$

where $\langle\cdots\rangle$ implies averaging over all phases $\delta_{\mathbf{q},\hat{\boldsymbol{\epsilon}}}$ which are assumed to be independent of one another. Furthermore, these phases do not influence the energy of a given displacement, which can be written as $E(\{n_{\mathbf{q},\hat{\boldsymbol{\epsilon}}}\})$. The experimentally-measured current is then calculated as a thermal average over all sets $\{n_{\mathbf{q},\hat{\boldsymbol{\epsilon}}}\}$, and can be written as

$$I(\mathbf{k}^f,E,T)=\frac{1}{Q(T)}\sum_{\{n_{\mathbf{q},\hat{\epsilon}}\}} I(\mathbf{k}^f,E,\{n_{\mathbf{q},\hat{\epsilon}}\}) \times\exp[-E(\{n_{\mathbf{q},\hat{\epsilon}}\})/k_BT] , \quad (7)$$

where k_B is Boltzmann's constant, T is the temperature, and $Q(T)$ is the vibrational partition function. The temperature-dependent sum on $\{n_{\mathbf{q},\hat{\epsilon}}\}$ is thus also a sum over all lattice displacements $\mathbf{U}_l$.

The exact evaluation of Eq. (6) thus requires initial-state energies and wave functions for each displaced lattice, a calculation of prohibitive difficulty. In order to make this evaluation more tractable, the following assumptions are made.[24] (1) The E^i's are assumed to be those of the equilibrium lattice. For Cu over the full 900 K range of interest here, this assumption is not expected to produce more than ~ 0.20 eV errors in E^i values.[5(a)] (2) The displacement-induced changes in the ψ^i's are assumed to be limited to phase differences between points which, in the equilibrium lattice, are related by a lattice translation vector, with that portion of ψ^i inside of a muffin-tin-like region around each nucleus translating rigidly with the nucleus and being otherwise unaffected. Within a muffin-tin radius r_{MT} approximately equal to $\frac{1}{2}$ of the nearest-neighbor distance in the displaced lattice, it is thus assumed that $\psi^i_{\mathbf{k}^i}(\mathbf{R}_n+\mathbf{r})$ equals, to within a phase factor, $\psi^{i(0)}_{\mathbf{k}^i}(\mathbf{R}^{(0)}_n+\mathbf{r})$. Thus, the emphasis is on phase changes which affect the $\mathbf{k}$ conservation properties of the optical matrix elements, and is analogous to the so-called "intra-atomic" effects discussed by Shevchik.[2(c)] (3) By analogy with the phase relationship between two sites n and l for initial states in the equilibrium lattice

$$\psi^i_{\mathbf{k}^i}(\mathbf{R}_n+\mathbf{r})=\exp[i\mathbf{k}^i\cdot(\mathbf{R}_n-\mathbf{R}_l)]\psi^i_{\mathbf{k}^i}(\mathbf{R}_l+\mathbf{r}) . \quad (8)$$

(4) The final states ψ^f are taken to be free-electron-like [or somewhat more accurately as single orthogonalized plane waves (OPW's)] with $E=E^f=\hbar^2(k^f)^2/2m$. In forming the OPW, the rigid translation of ψ^i (to within a phase change) is again taken into account. (5) The displaced-lattice matrix elements analogous to those in Eq. (3) are assumed to be dominated by the region inside of r_{MT}, a result which can be argued by converting to the potential gradient form of the dipole operator, and which is also expected to be more and more valid as energy is increased.[34]

With these assumptions, the equivalent of the optical matrix element of Eq. (3) for the displaced lattice becomes

$$M_{if}(\mathbf{k}^f,\mathbf{k}^i)=\frac{1}{\omega}m^{(0)}_{if}(\mathbf{k}^f,\mathbf{k}^i)\sum_{\mathbf{R}_l}\exp[-i\,\Delta\mathbf{k}\cdot(\mathbf{R}^{(0)}_l+\mathbf{U}_l)] , \quad (9)$$

where $\Delta\mathbf{k}=\mathbf{k}^f-\mathbf{k}^i$, and $m^{(0)}_{if}$ is evaluated within a single typical muffin tin and with ψ's for the equilibrium lattice as

$$m^{(0)}_{if}(\mathbf{k}^f,\mathbf{k}^i)=\int_{|\mathbf{r}-\mathbf{R}^{(0)}_l|<r_{\mathrm{MT}}} d^3r\,\psi^{f(0)*}_{\mathbf{k}^f}(\mathbf{r})\mathbf{A}\cdot\nabla V(\mathbf{r}) \times\psi^{i(0)}_{\mathbf{k}^i}(\mathbf{r}) . \quad (10)$$

We have here implicitly neglected the photon wave vector $\mathbf{k}_{h\nu}$ as being small in comparison to $\mathbf{k}^f$ and $\mathbf{k}^i$ at the photon energies of relevance here. (This is *not* true in the XPS limit, however.[6]) Expanding Eq. (9) in powers of the individual mode displacements $\mathbf{U}_{l,\mathbf{q},\hat{\epsilon}}$ from Eq. (4a), we have

$$M_{if}(\mathbf{k}^f,\mathbf{k}^i)=\frac{1}{\omega}m^{(0)}_{if}(\mathbf{k}^f,\mathbf{k}^i)\sum_{\mathbf{R}_l}\exp(-i\Delta\mathbf{k}\cdot\mathbf{R}^{(0)}_l)\prod_{\substack{\mathbf{q},\hat{\epsilon}\\ \mathbf{q}\neq 0}}[1-i\,\Delta\mathbf{k}\cdot\mathbf{U}_{l,\mathbf{q},\hat{\epsilon}}-\tfrac{1}{2}(\Delta\mathbf{k}\cdot\mathbf{U}_{l,\mathbf{q},\hat{\epsilon}})^2+\cdots] . \quad (11)$$

This can be rewritten in terms of the phonon amplitudes $A_{\mathbf{q},\hat{\epsilon}}$ by using Eq. (4b). After some manipulation, this becomes

$$M_{if}(\mathbf{k}^f,\mathbf{k}^i)=\frac{N}{\omega}m^{(0)}_{if}(\mathbf{k}^f,\mathbf{k}^i)\sum_{m=0}^{\infty}\sum_{\{m^{\pm}_{\mathbf{q},\hat{\epsilon}}\}}^{m}\delta(\mathbf{k}^f-\mathbf{k}^i-\mathbf{g}-\mathbf{Q})\left[\prod_{\substack{\mathbf{q},\hat{\epsilon}\\ \mathbf{q}\neq 0}}\frac{1}{m^+_{\mathbf{q},\hat{\epsilon}}!m^-_{\mathbf{q},\hat{\epsilon}}!}\left(-\frac{i}{2}A_{\mathbf{q},\hat{\epsilon}}\hat{\epsilon}\cdot\Delta\mathbf{k}\right)^{m^+_{\mathbf{q},\hat{\epsilon}}+m^-_{\mathbf{q},\hat{\epsilon}}} \times\exp[i(m^+_{\mathbf{q},\hat{\epsilon}}-m^-_{\mathbf{q},\hat{\epsilon}})\delta_{\mathbf{q},\hat{\epsilon}}]\right] , \quad (12)$$

where $m^+_{\mathbf{q},\hat{\epsilon}}(m^-_{\mathbf{q},\hat{\epsilon}})$ is the number of phonons of mode $\mathbf{q},\hat{\epsilon}$ absorbed (emitted) in a given photoexcitation event; m is the overall order of the phonon involvement, such that, for a given set $\{m^{\pm}_{\mathbf{q},\hat{\epsilon}}\}$,

$$m=\sum_{\mathbf{q},\hat{\epsilon}}(m^+_{\mathbf{q},\hat{\epsilon}}+m^-_{\mathbf{q},\hat{\epsilon}}) ; \quad (13)$$

the inner summation is on all sets $\{m^{\pm}_{\mathbf{q},\hat{\epsilon}}\}$ yielding a given m; and $\mathbf{Q}$ is the total phonon wave-vector contribution to $\mathbf{k}$ conservation, as given by

$$\mathbf{Q}=\sum_{\mathbf{q},\hat{\epsilon}}(m^+_{\mathbf{q},\hat{\epsilon}}-m^-_{\mathbf{q},\hat{\epsilon}})\mathbf{q} . \quad (14)$$

Wave-vector conservation is thus modified to

$$\mathbf{k}^f=\mathbf{k}^i+\mathbf{g}+\mathbf{Q} , \quad (15)$$

(cf. Fig. 1), and all possible combinations of phonon absorption (emission) events are included in Eq. (12), in

which they are grouped by order for convenience.

The total photocurrent at finite T can then be evaluated by replacing $M_{if}^{(0)}$ in Eq. (3) with M_{if} from Eq. (12), and then carrying out the phase and thermal averages of Eqs. (6) and (7). From this, with some manipulation one can extract direct- and non-direct-transition components, and determine their respective temperature dependences.[24] We separately consider the end results of this analysis for the two components.

For direct transitions, $\mathbf{Q}=0$ in Eq. (15) and various phonon absorptions and emissions may be involved, as long as they yield this value. In general, this requires that $m^{+}_{\mathbf{q},\hat{\epsilon}}=m^{-}_{\mathbf{q},\hat{\epsilon}}$ for all modes involved. In the limit of large N, simplifications occur in the phase averaging, and the direct-transition matrix element from Eq. (12) becomes

$$\langle M_{if}(\mathbf{k}^f,\mathbf{k}^i)\rangle_{\text{phase}} = \frac{N}{\omega} m_{if}^{(0)}(\mathbf{k}^f,\mathbf{k}^i) \exp\left[-\tfrac{1}{4}\sum_{\substack{\mathbf{q},\hat{\epsilon}\\ \mathbf{q}\neq 0}} A^2_{\mathbf{q},\hat{\epsilon}}(\hat{\epsilon}\cdot\Delta\mathbf{k})^2\right], \quad (16)$$

where $\Delta\mathbf{k}=\mathbf{k}^f-\mathbf{k}^i=\mathbf{g}$. Using this result to express $I(\mathbf{k}^f,E,\{n_{\mathbf{q},\hat{\epsilon}}\})$ in Eq. (6) and then calculating $I(\mathbf{k}^f,E,T)$ from Eq. (7) shows that the thermal average of the square of the exponential in Eq. (16) is precisely the usual Debye-Waller factor as discussed elsewhere:[2(b),26]

$$W(T)=\exp\left[-\tfrac{1}{2}\sum_{\mathbf{q},\hat{\epsilon}}(\hat{\epsilon}\cdot\Delta\mathbf{k})^2\langle A^2_{\mathbf{q},\hat{\epsilon}}\rangle\right], \quad (17)$$

where $\langle A^2_{\mathbf{q},\hat{\epsilon}}\rangle$ is the thermal average of $A^2_{\mathbf{q},\hat{\epsilon}}$ over all $n_{\mathbf{q},\hat{\epsilon}}$, as given by Eq. (5) with $n_{\mathbf{q},\hat{\epsilon}}$ replaced by

$$\langle n_{\mathbf{q},\hat{\epsilon}}\rangle=\frac{1}{\exp(\hbar\omega_{\mathbf{q},\hat{\epsilon}}/k_BT)-1}. \quad (18)$$

Thus, Eq. (7) finally yields an expression for the direct-transition photocurrent of the form

$$I_{\text{DT}}(\mathbf{k}^f,E,T)=W(T)I^{(0)}_{\text{DT}}(\mathbf{k}^f,E), \quad (19)$$

where $I^{(0)}_{\text{DT}}(\mathbf{k}^f,E)$ is the DT component of the photocurrent in the equilibrium lattice, as given by

$$I^{(0)}_{\text{DT}}(\mathbf{k}^f,E)\propto v\sum_i \delta(E-E^i-\hbar\omega)\delta(\mathbf{k}^f-\mathbf{k}^i-\mathbf{g}) \times |M^{(0)}_{if}(\mathbf{k}^f,\mathbf{k}^i)|^2. \quad (20)$$

This result is thus identical in form to the first term of Eq. (1).

A similar analysis of the non-direct-transition component for which $\mathbf{Q}\neq 0$ yields a result of much greater complexity. The final form of the phase average of the NDT matrix element squared is

$$\langle |M_{if}(\mathbf{k}^f,\mathbf{k}^i)|^2\rangle_{\text{phase}}=\frac{N^2}{\omega^2}|m^{(0)}_{if}(\mathbf{k}^f,\mathbf{k}^i)|^2\exp\left[-\tfrac{1}{2}\sum_{\substack{\mathbf{q},\hat{\epsilon}\\ \mathbf{q}\neq 0}} A^2_{\mathbf{q},\hat{\epsilon}}(\hat{\epsilon}\cdot\Delta\mathbf{k})^2\right]\sum_{\{m^{\pm}_{\mathbf{q},\hat{\epsilon}}\}}\delta(\mathbf{k}^f-\mathbf{k}^i-\mathbf{g}-\mathbf{Q})|[\cdots]|^2, \quad (21)$$

where $[\cdots]$ is the product in large square brackets on the right-hand side of Eq. (12), and the δ function in $\mathbf{k}$ implies summing only on the set $\{m^{\pm}_{\mathbf{q},\hat{\epsilon}}\}$ for which $\mathbf{k}^i$ can be coupled to $\mathbf{k}^f$ via some $\mathbf{Q}$ and some $\mathbf{g}$. The final result for the non-direct current is then found to be

$$I_{\text{NDT}}(\mathbf{k}^f,E,T)\propto\frac{vN^2}{\omega^2}\sum_i\delta(E-E^i-\hbar\omega)W_i(T)|m^{(0)}_{if}|^2\sum_{\{m^{\pm}_{\mathbf{q},\hat{\epsilon}}\}}\delta(\mathbf{k}^f-\mathbf{k}^i-\mathbf{g}-\mathbf{Q})\langle|[\cdots]|^2\rangle, \quad (22)$$

where $W_i(T)$ depends on $\mathbf{k}^i$ through $\Delta\mathbf{k}=\mathbf{k}^f-\mathbf{k}^i=\mathbf{g}+\mathbf{Q}$. Combining Eqs. (19) and (22) thus yields as the total current:

$$I(\mathbf{k}^f,E,T)=W(T)I^{(0)}_{\text{DT}}(\mathbf{k}^f,E)+I_{\text{NDT}}(\mathbf{k}^f,E,T), \quad (23)$$

in which the temperature dependence of I_{NDT} is considerably more complex than Eq. (1).

At this point, we can also ask whether phonons of the proper symmetry (symmetries) can participate in an excitation such that an $i\rightarrow f$ transition which is symmetry forbidden in the equilibrium lattice will become allowed. Within the model discussed here, this cannot occur, since the prefactor $|m^{(0)}_{if}|^2$ in Eq. (22) contains information on the symmetry of the equilibrium lattice, and will thus be zero for such transitions. In more general models of such phonon-assisted transitions, such a transition might become allowed, however.

If only single-phonon processes for which $m=1$ are considered, such that $\mathbf{Q}=\pm\mathbf{q}$, then Eq. (22) can be simplified to

$$I^{(1)}_{\text{NDT}}(\mathbf{k}^f,E,T)\propto\frac{vN^2}{\omega^2}\sum_i\delta(E-E^i-\hbar\omega)|m^{(0)}_{if}|^2\sum_{\mathbf{q},\hat{\epsilon}}\delta(\mathbf{k}^f-\mathbf{k}^i-\mathbf{g}-\mathbf{q})\tfrac{1}{2}\langle A^2_{\mathbf{q},\hat{\epsilon}}\rangle(\hat{\epsilon}\cdot\Delta\mathbf{k})^2, \quad (24)$$

where $\langle A^2_{\mathbf{q},\hat{\epsilon}}\rangle$ is calculated as in Eqs. (17) and (18), but now used in a much more restricted summation. This result is similar to, but not identical to, a first-order I_{NDT} derived by Shevchik via a more approximate treatment of phonons [Eq. (18) in Ref. 2(b)]. If we additionally assume that $|m^{(0)}_{if}|^2$ is constant and let $\Delta\mathbf{k}=\mathbf{g}$, then a comparison of Eqs. (24) and (17) also shows that, to first order in the exponent of the Debye-Waller factor the total photo-

current equals $I_{DT}(1-\omega)/W$. Our results for this very special case are thus consistent with Eq. (1).

Although the multiple BZ sums involved in Eq. (22) make full-order calculations of I_{NDT} via this model extremely difficult, several useful qualitative conclusions can be drawn from this analysis.[24]

(1) The values of $\langle A^2_{\mathbf{q},\hat{\epsilon}} \rangle$ controlling the contribution of a given mode fall off very rapidly as q increases from zero. Therefore, the NDT intensity is expected to be peaked about the DT value for $\mathbf{k}^i$, a point mentioned also by Shevchik via his first-order analysis[2(b)] and a result familiar in x-ray[26] and electron[27] diffraction. For example, an estimate of this peaking for Cu at 300 K based upon the first-order Eq. (24) and the Debye model indicates that $\sim 50\%$ of the nondirect transitions will originate in a region centered on the direct transition that is only 14% of the BZ volume. Thus, it is expected that NDT effects alone may cause different DT peaks to show different temperature behavior, depending for example, upon whether the bands in that region of $\mathbf{k}^i$ are strongly dispersive or not. This conclusion thus supports some of our earlier comments concerning the data in Figs. 3—9. By analogy with x-ray diffraction, such NDT's may not be isotropically distributed about the DT $\mathbf{k}^i$,[26(b)] although we will later assume this for simplicity.

(2) Expanding the Debye-Waller factor in powers of its argument yields $(-\frac{1}{3}\overline{U^2}g^2)^n/n!$ as an estimate of the relative importance of nth order processes, and suggests that terms up to approximately $n=2$—3 may have to be included over the temperature range of our data for Cu.

(3) Comparison of Eqs. (1) and (23) also indicates that the use of temperature-dependent data and Eq. (1) to deconvolute spectra so as to obtain DT and NDT components is not rigorous, and may result in the inclusion of some NDT intensity in the empirical DT components so derived. This has, in fact, been seen in recent ARXPS studies.[6,25] Such an analysis also was not found to give reasonable I_{NDT} curves for the present Cu data, and it will not be used here.

In order to semiquantitatively model the effects of such nondirect transitions on spectra, we have chosen a very simple model in order to avoid entirely the complex phonon sums of the previous analysis. This involves incorporating a cylindrical BZ broadening centered on $\mathbf{k}^i$ in a simple DT calculation with constant matrix elements. Such cylinders including phonon contributions are shown in Fig. 1, and they have been arbitrarily increased in radius and length by equal amounts around a "core" cylinder of minimum broadening due to the finite angular acceptance of the analyzer and electron inelastic attenuation. These minimum inner cylinders also are shown in Fig. 1, with a radius $\Delta k^f_{\perp,\min}$ perpendicular to $\mathbf{k}^f$ determined by the angular acceptance of the analyzer,[6,20,35] and a half-length of $\Delta k^f_{||,\min}$ parallel to $\mathbf{k}^f$ determined by the inelastic attenuation length Λ_e. The dimensions of these inner cylinders are drawn to scale according to the values finally chosen to represent this minimum broadening, and it is clear that Λ_e broadening is more important for the present case. From 500 to 30000 $\mathbf{k}$ points were included in these broadenings, depending upon the cylinder size.

The angular broadening due to the analyzer angular acceptance is assumed to be associated with a cone of $\Delta\theta = 1.0°$ half angle. This yields a relatively small inner cylinder radius of $\Delta k^f_{\perp,\min} = k^f \tan\Delta\theta$ of 0.035—$0.052(2\pi/a)$ between $h\nu = 40$ and 106 eV, respectively, and, if anything, may somewhat overestimate this effect, which is quite small in any case.

The choice for minimum broadening induced by Λ_e cannot be made as precisely as that for angular resolution. A generally accepted estimate for this value based upon the uncertainty principle is $\Delta k^f_{||,\min}$ (defined to be $\frac{1}{2}$ of the overall $\pm$ broadening) $\approx 1/2\Lambda_e$.[6,33] In the energy regime of relevance here, the Λ_e for Cu is at its minimum, and previously reported values lie between ~ 3.0 and ~ 7.0 Å, but with more weight toward 5.0—7.0 Å.[36] This yields $\Delta k^f_{||,\min}$ values of between $0.06(2\pi/a)$ and $0.04(2\pi/a)$, respectively. However, if the decay of intensity due to inelastic scattering is exponential, then a better estimate of $\Delta k^f_{||,\min}$ is perhaps obtained from one-half of the FWHM in k of the Fourier transform of $\exp(-l/\Lambda_e)$, where l is path length. A recent analysis of Fourier transform methods by Barton and Shirley[37] shows this criterion to be

$$\Delta k^f_{||,\min} = \pi(0.55)/\Lambda_e \ ,$$

or a value approximately 3.5 times those obtained using $1/2\Lambda_e$. However, we have for Cu(100) found little sensitivity to the value of $\Delta k^f_{||,\min}$ used, especially as additional isotropic broadening for phonons is needed to adequately describe our data. Hence all calculations for Cu(001) discussed here have been performed with

$$\Delta k^f_{||,\min} = (\pm 0.15 - \pm 0.16)(2\pi/a) \ ,$$

which would correspond to $\Lambda_e \approx 2.0$ Å if derived from $1/2\Lambda_e$, or to ~ 6.4 Å if derived from the Fourier-transform method. If anything, this is probably a slight overestimate of this contribution as well, and a smaller Λ_e broadening is in fact suggested from an analysis of Cu(011) experimental data that is discussed below.

Additional broadening due to phonons was simulated by incrementing the cylinder size in both radius and half-length by the same amount, usually $0.05(2\pi/a)$ or $0.10(2\pi/a)$.

A final Gaussian energy broadening of 0.2 eV FWHM has been performed on each calculated spectrum to simulate overall instrumental energy resolution. We have neglected any energy broadening due to the hole lifetime, although this might be expected to yield a variable additional contribution to width from zero at E_F to ~ 1 eV at the bottom of the bands.[23] However, this added broadening would not depend strongly on temperature, and thus would not affect any of our conclusions.

As input for the initial state $E^i, \mathbf{k}^i$ values for Cu, we have used the band structure calculated by Burdick[30] and shown in Fig. 2. A comparison of photoemission results for Cu(001) and Cu(011) with available band structures has shown[20,23,38] that there is, in general, better agreement with Burdick's non-self-consistent augmented plane-wave calculation than with more recent self-consistent band-structure calculations,[39] although the differences among

these calculations are usually $\lesssim 0.05$ eV. (Possible spin-orbit splittings near the center of the zone[39] are expected to be $\lesssim 0.2$ eV and not to show temperature dependence; thus they should not affect any of our later conclusions.) Similar calculations for ferromagnetic Ni are discussed in a later section.

C. Comparison of cylindrically-broadened DT theory to experiment

1. Data for Cu(001)

Direct transition calculations for Cu are shown in Fig. 10 for $h\nu=41$ eV and DT emission from the Γ point. The calculated spectrum with only minimal broadening to account for angular resolution and Λ_e is shown in Fig. 10(g). It is clear in comparison with the 77 K experimental result of Fig. 7(d) that, although major peak positions are well predicted, angular broadening and Λ_e broadening are not by themselves enough to account for the widths and shapes of the direct-transition peaks. This is in spite of the fact that the Debye-Waller factor suggests that $\sim 98\%$ of the transitions should be direct. Although peak positions are correctly predicted (with the exception of the weak s-p band intensity below 8 eV that arises from the bottom of the Δ_1 band) the depth of the valley between the experimental peaks a and b is much more shallow than that between a' and b' in the calculation. In addition, a shoulder appears on feature b in the experimental spectrum which is not present in the calculation of Fig. 10(g). As temperature is increased in Figs. 7(c)—7(a), the valley between a and b fills in and the spectrum widens as phonon contributions increase. The shoulder on the low-energy side of b gains intensity while the clear resolution of a is lost. There is also a smearing and reduction of the intensity at 6 to 8 eV from the steeply dispersing Δ_1 band. All of these qualitative trends are reproduced in the calculations as the amount of isotropic cylindrical broadening is increased with an arbitrary step size of $0.1(2\pi/a)$ in Figs. 10(f) through 10(a). The only differences are a slower buildup of intensity between 0 and 2 eV in theory, and a larger relative peak height a'/b' than observed. The former may be due to inadequacies in our cylindrical broadening, such that the "wings" of the true NDT distribution in $\mathbf{k}^i$ bring in more s-p intensity in this energy region. For the latter, we have noted previously that the assumption of constant matrix elements in the calculation does not allow for the symmetry of the bands sampled. Thus, since a' is largely Δ_5 in origin (and weak due to the experimental geometry) and b' is of Δ_1 origin (and emphasized by the experimental geometry) the disparity between a'/b' and a/b is easily explained.

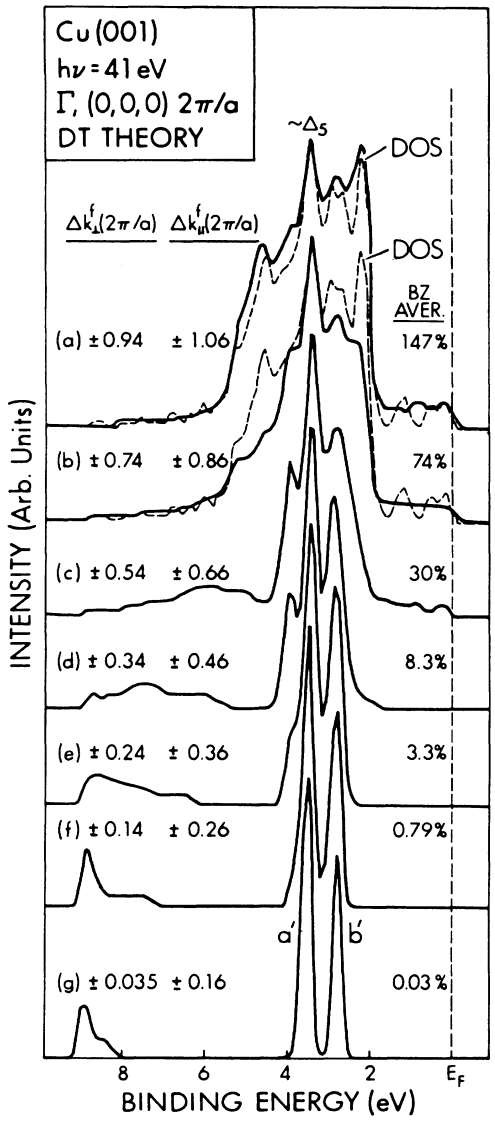

FIG. 10. Theoretical Γ-point spectra with different degrees of cylindrical broadening as defined by $\Delta k_\perp^f$ and $\Delta k_\parallel^f$ (cf. Fig. 1). Also shown is the percentage of the BZ volume averaged over in each case, and the total DOS (as dashed curves).

Empirically matching the calculations of Fig. 10 to the spectra of Fig. 7 at various temperatures, we find that the 77 K spectrum of Fig. 7(d) is best reproduced by the DT calculations of Fig. 10(e) or 10(f). The latter correspond to a broadening over only 0.79—3.3 % of the BZ, but the overall peak widths, the overall depth of the valley between a and b, and the intensity from 6—8 eV are all very well described and certainly in much better agreement with experiment than with minimal broadening. Note also the very rapid smearing and shifting to lower binding energy of the Δ_1-derived intensity at 6—9 eV, even with only a few percent BZ broadening. Thus, even at 77 K and with a W of 0.98 suggesting only $\sim 2\%$ NDT intensity, the presence of significant effects due to such NDT broadening is suggested. This result is also consistent with the notion of an effective $W(T)$ which is smaller than the bulk value due to increased $\overline{U^2}$ values at the surface, a point to which we will return in greater detail below.

Proceeding with comparison of experiment to theory for $h\nu=41$ eV, we find that the room-temperature data [Fig. 7(c)] agree best with broadening in the range of Fig. 10(d) or 10(e), corresponding to averaging over 3.3—8.3 % of the BZ. At 793 K, experiment in Fig. 7(b) agrees best

with Fig. 10(c) or 10(d), corresponding to 8.3—30% BZ averaging. As noted previously, the high-temperature limit of 973 K for the experiment in Fig. 7(a) does not approach the DOS [cf. dashed curve in Fig. 10(a)], but this is perhaps not surprising as $W(T)$ is still reasonably large at 0.79. The best overall agreement for this case is with Fig. 10(c) or ~30% BZ averaging. At first sight it might not seem reasonable in the theoretical curves that averaging over $\gg \frac{1}{48} = 2.1\%$ of the BZ (the volume in **k** space of an irreducible wedge) does not result in a calculated spectrum which is essentially the DOS. This is due to the fact that, as the broadening volume is increased, different portions of adjacent wedges are sampled and, in general, the sampling is nonuniform over a given wedge. Thus, one must approach > 100% BZ averaging before reaching DOS-like behavior in predicted spectra.

In Fig. 11, broadened DT calculations for $h\nu = 81$ eV are presented. In comparing these with the experimental data of Fig. 8, particular points of interest are the temperature-dependent shifts of peak *c* and shoulder *d*. However, the calculations do not attempt to include umklapp processes and so are not expected to represent features *d* and *e* well, particularly at lower temperatures.

Comparing the 77 K spectrum of Fig. 8(c) to theory yields the best agreement with the curve of Figs. 11(d) and 11(e) corresponding to 3.4—8.7% BZ broadening. This match is based primarily on the position of peak *c*, but this degree of BZ averaging also appears to account for a significant amount of intensity near shoulder *d* in the experimental data. The shift of *d* to higher binding energy for higher temperatures can also be explained with increases in the degree of BZ averaging. The 295 K experimental data of Fig. 8(b) are found to match theory best for broadening somewhere between Figs. 11(d) and 11(c) or 8.7—17.5% of the BZ. The shift of peak *c* between 77 and 295 K is also well explained by these choices of broadenings. At 973 K, a broadening between Figs. 11(c) and 11(b) or between 17.5—31% yields optimum agreement, although the general smearing of features and the possible influence of the Γ umklapp makes this a more approximate estimate.

Figure 12 shows broadened DT calculations for $h\nu = 97$ eV, in the same format as Figs. 10 and 11. Comparison of the minimally broadened calculations of Fig. 12(f) with Fig. 9(c) immediately indicates some significant differences between theory and low-temperature experiment. First, the peak at ~4.8 eV in theory is not seen in experiment due to its forbidden Δ_2' character. Also, the peak *j'*

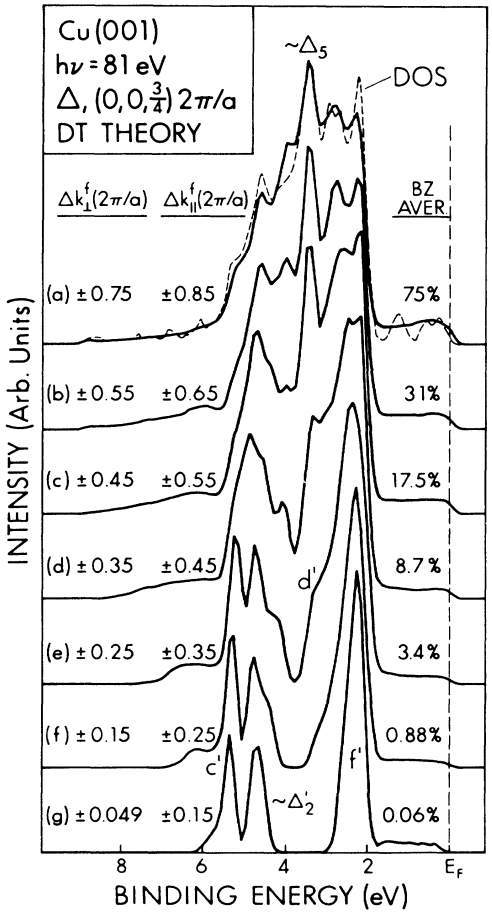

FIG. 11. Same as Fig. 10, but for $h\nu = 81$ eV and Δ-point emission.

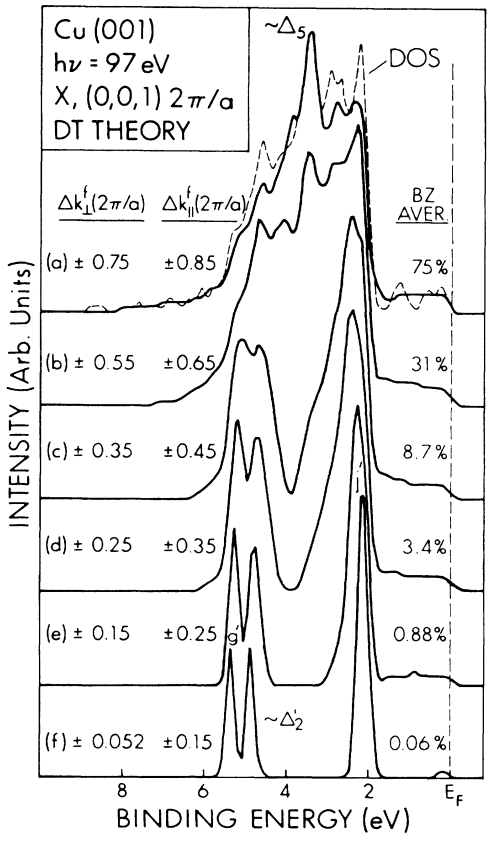

FIG. 12. Same as Fig. 10, but for $h\nu = 97$ eV and *X*-point emission.

is expected to be weak due to its Δ_5 character (cf. Fig. 2). Allowing for these effects, a cylindrical broadening to greater than 8.7% is required to produce enough intensity in the valley between j' and g' to approximately match Fig. 9(c). However, as discussed previously, intensity in the experiment at h and i has been suggested to be a result of an umklapp process involving the surface reciprocal-lattice vector $\mathbf{g}_s=(0,2,0)2\pi/a$.[23(b)] Allowing for this umklapp process [cf. dashed curve in Fig. 9(c)] now shows that calculations for 0.88% to 3.4% BZ averaging are the best match for $h\nu=97$ eV and $T=77$ K; this match is based primarily on the position of peak g and the s-p band intensity for 0—1.7 eV. For $T=295$ K in Fig. 9(b), the best empirical match is obtained for cylindrical broadenings over 3.4—8.7% of the BZ, and the $T=977$ K spectrum matches well with averaging over $\sim$30% of the BZ, as this is the minimum required to totally fill in the valley between g' and j'. These empirical broadenings at different temperatures are thus consistent with the values obtained for $h\nu=41$ and 81 eV. The $T=977$ K spectrum for emission from X still does not look like the DOS [cf. dashed curve in Fig. 12(a)], and comparison to the corresponding high-temperature Γ spectrum [dashed curve in Fig. 9(a)] suggests a strong umklapp contribution at high temperature as well. In fact, the umklapp-dominated peak at the position of i appears to be stronger than the DT peak j over the full temperature range. There is, however, a 0.2 eV shift of this main peak to lower energy in the X-point spectra at high temperature as compared to the corresponding Γ-point spectrum.

Comparisons of experiment and broadened DT theory analogous to those in Figs. 7 and 10, 8 and 11, and 9 and 12 have been made for all of the other energies studied (that is, 53, 66, 89, and 106 eV). With allowance for Γ umklapp intensity for $h\nu\geq 66$ eV, it is in all cases found to be possible to well describe the general evolution of features as temperature is increased. Overall, the amounts of BZ averaging required are reasonably consistent as well, being $\sim$1—3% at 77 K, $\sim$3—9% at 295 K, $\sim$9—20% at 793 K, and $\sim$20—30% at 973 K. Quite importantly, the peak positions and shifts for both $h\nu=66$ eV and $h\nu=81$ eV (cf. Figs. 8 and 11) on going from 77 to 295 K are both very well produced by the DT calculations with roughly the same degree of averaging; for 66 eV matching the observed position of peak c to theory yields $\sim$3% at 77 K and $\sim$8% at 295 K, and for 81 eV these numbers are $\sim$6% and $\sim$13%, respectively.

It is also appropriate to comment here on a method that is somewhat similar to ours for calculating the photocurrent from solids, as first suggested by Grandke *et al.* for PbS (Ref. 40) and later discussed by Ley (Ref. 41). This so-called weighted indirect-transition model or weighted one-dimensional density-of-states model has been found to work very well for PbS, PbSe, and PbTe, but not as well for other materials. In this model, it is assumed that $k_{\parallel}$ conservation exists, but that all values of $k_\perp$ may contribute to the photoemission spectrum. The photocurrent so derived is then found to be $\propto(dE^i/dk_\perp^i)^{-1}$ such that singularities in the band structure along $k_\perp$ would contribute most strongly. The resulting one-dimensional DOS is then modulated by a weighting factor which has a maximum at $k_\perp^i=\mathrm{Re}(k_\perp^f)$ and drops off on either side with a width determined by $\mathrm{Im}(k_\perp^f)\propto 1/\Lambda_e$. For $\mathrm{Im}(k^f)\rightarrow 0$, the weighting factor is thus a δ function corresponding to infinite Λ_e and complete conservation of $k_\perp$. For very short Λ_e, the spectrum will arise from the one-dimensional DOS. This model is thus very close to ours in the limit of $\Delta k_{\parallel}^f\gtrsim 2\pi/a$ and $\Delta k_\perp^f\approx 0$, except that ours includes no weighting factor. One major result of this model is that certain peaks originating from singularities in the DOS along $k_\perp$ [as flat regions for Cu(001) like a', b' for Γ in Fig. 2] will contribute very strongly and will not shift in position as $h\nu$ is varied. Thiry[23(b)] has attributed some spectral features from Cu(001) and Cu(011) to this kind of contribution, an example of which is the shoulder on peak b in Fig. 7. We have found that with high angular resolution and $T=77$ K, no such one-dimensional DOS peaks need to be invoked to explain our results for Cu(001) as $h\nu$ is varied, and that a three-dimensional cylindrical broadening can as well account for peaks which at first glance appear to have no origin in the band structure. In an attempt to incorporate a more physically reasonable nonuniform weighting in our model, we have also carried out a series of calculations incorporating Gaussian weightings in both the $k_\perp^f$ and $k_{\parallel}^f$ directions. These to first order would approximate the expected peaking of the nondirect transitions about $\mathbf{k}^i$, as well as the weighting factors in the one-dimensional DOS model. These results were, in general, in poorer agreement with experiment, and also did not converge as quickly to the correct three-dimensional DOS limit for large degrees of BZ averaging.

2. *Data for Cu(011)*

In view of the success of the simple, cylindrically-broadened DT model in describing a number of features of the temperature dependence of our data for Cu(001), we have also attempted to describe the data of Williams *et al.*[3] for Cu(011) in the same manner. Figure 13 shows this temperature-dependent data for $h\nu=45$ eV with the normal-emission geometry in the inset, together with our corresponding DT calculations. The bulk Debye-Waller factors are again given, with values in agreement with those quoted previously[3] and also somewhat smaller than those for Cu(001) due to the larger $\mathbf{g}$ vector of $(0,2,2)2\pi/a$ involved. Here, as noted originally by Williams *et al.*, the most striking aspect is the very rapid smearing and loss in relative intensity of the s-p derived peak d at $\sim$0.6 eV as temperature is increased, even from 298 and 473 K. This peak is exceptionally strong in view of the fact that such s-p bands are, in general, expected to have much lower matrix elements than d-band states.[42,43] The strength of this peak has been attributed to some sort of resonance effect,[3] and it is apparent that raising the temperature quickly shifts this feature to higher binding energy and suppresses it relative to the d-band associated features a—c below it. Our results for Cu(001) at 77 and 295 K also make it clear that analogous low-temperature data for Cu(011) should be extremely interesting, probably exhibiting a much sharper and more intense resonance.

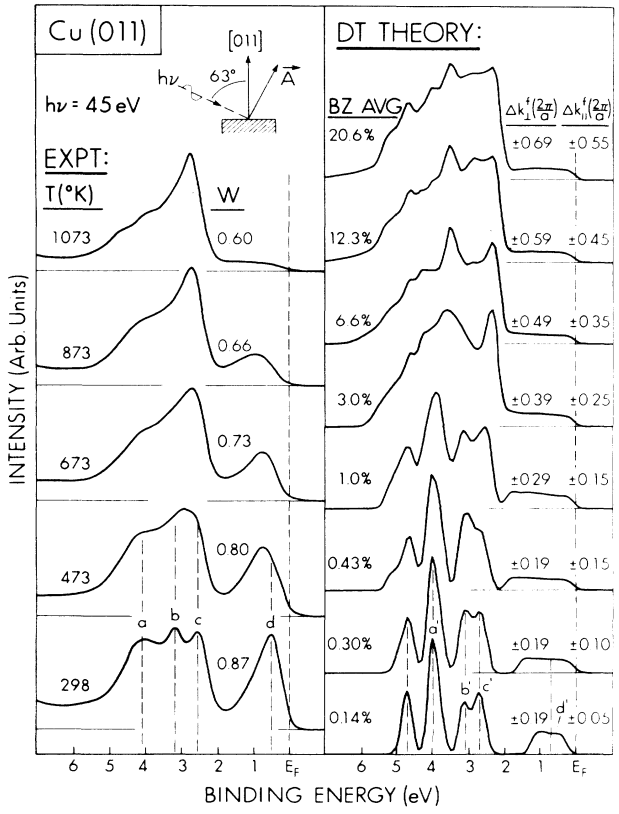

FIG. 13. The left panel shows experimental normal-emission spectra for Cu(011) obtained by Williams *et al.* (Ref. 3) for $h\nu=45$ eV and temperatures of 298–1073 K. The experimental geometry is shown in the inset. The right panel shows cylindrically-broadened direct-transition calculations as in Figs. 10, 11, and 12, except that the minimum values of $\Delta k_{\perp}^{f}$ and $\Delta k_{\parallel}^{f}$ have been adjusted slightly, as discussed in the text.

The right panel of Fig. 13 attempts to model these data with cylindrically-broadened DT calculations. In this case, the angular resolution was taken to be $\pm 4° \times \pm 6°$,[44] yielding an assumed angular acceptance cone of $\pm 5°$ and a relatively large value for $\Delta k_{\perp,\min}^{f}$ of $0.19(2\pi/a)$. These calculations were found to be more sensitive to the choice of Λ_e broadening via $\Delta k_{\parallel,\min}^{f}$ than those for Cu(001). In order to predict a reasonably sharp feature corresponding to peak d in the calculations, a reduced value of $\Delta k_{\parallel,\min}^{f}=0.05(2\pi/a)$ had to be used. This is due to the very high dispersion of the Σ_1 band involved (very much like Δ_1 near E_F in Fig. 2). [Comparison to Fig. 10 at comparable energy thus suggests that our minimum "core" of BZ averaging for Cu(001) was perhaps too large, although for this case, additional effective broadening due to phonon effects is strong enough even at 77 K that none of our earlier conclusions are affected.]

Comparing experiment and theory in Fig. 13, we see good agreement as to general trends with increasing temperature. At 298 K, the positions of features a–d are rather well reproduced by features a'–d' in the minimally-broadened theory. The resonance peak d is narrower and sharper than d', but its position is predicted very well. This additional sharpness may suggest an even lower effective **k** broadening in experiment, particularly in the case of $\Delta k_{\perp}^{f}$. Specifically, $\Delta k_{\perp,\min}^{f}$ could be lower than expected due to a reduced effective angular acceptance caused by retardation losses in the cylindrical-mirror analyzer used. A peak at 4.7 eV in theory associated with a Σ_1 band is not seen in experiment, probably due to matrix-element effects. Also, peak a' is too strong relative to b' and c', again probably due to matrix elements. However, the temperature dependence in Fig. 13 is very well predicted by theory if such matrix-element effects on certain relative intensities are taken into account. The feature d' is quickly broadened and reduced in relative intensity as the degree of BZ averaging is increased, and by $\gtrsim 3.0\%$ averaging is fully smeared out in a manner fully consistent with the experimental curve at 1073 K. These rather dramatic effects predicted on the basis of near-**k**-conserving nondirect transitions thus may explain why fitting the temperature dependence of peak d to a simple Debye-Waller form was not found to describe the experimental data.[3]

One cause of the rapid loss in the intensity of peak d was attributed by Williams *et al.* to enhanced surfaced vibrations, effectively larger $\overline{U^2}$ values, and hence smaller Debye-Waller factors for the surface. This is reasonable since the majority of photocurrent is expected to come from the surface layer ($\Lambda_e \sim 5$ Å with $a_{\mathrm{Cu}}=3.6$ Å). Effects due to enhanced surface vibrations have also been suggested for Cu(111) by Mårtensson *et al.*,[9] who found it necessary to assign a lower effective Debye temperature Θ_D^{eff} to each peak, rather than to use a single effective Debye-Waller factor for the surface. This Θ_D^{eff} was strongly peak dependent, consistent with the result of the model we have been discussing in which NDT effects are expected to be strongly dependent on $\mathbf{k}^i$. Similar results have been found for Cu(110) (Refs. 10 and 11) and Ag(100) (Ref. 12). This sensitivity to $\mathbf{k}^i$ has also been attributed to modified surface dynamics and multiple scattering, and possible changes in ψ^i hybridization due to vibrational effects.[8,10] The effects of increased surface vibrations could be incorporated into the model of Eqs. (19), (20), and (22) by increasing the phonon amplitudes, perhaps to match experimental results. This would be seen in our simple DT model as effectively lower Debye-Waller factors for the surface and a greater degree of cylindrical BZ averaging at a given temperature than might be expected.

The same approach based on enhanced surface vibrations has been taken by Jezequel *et al.*,[13] who found that the temperature dependence of DT's from Pb(100) and Pb(110) for $20 \leq T \leq 400$ K could be reasonably well described by layer-averaged $W(T)$'s, with $\overline{U^2}$ for each layer being obtained from LEED measurements. They also have not noted significant differences in the temperature dependences (that is, the Θ_D^{eff} values) for different peaks. We have carried out a calculation similar to theirs for Cu(001), using bulk $\overline{U^2}$ values for all but the surface layer, and a surface $\overline{U^2}$ that is twice that of the bulk. The weighting of each layer was $\propto \exp[-z/\Lambda_e]$, where z is the perpendicular layer distance. This results in Debye-Waller factors for $h\nu=41$–97 eV and 295 K of $W=0.90$

if $\Lambda_e = 6.2$ Å is assumed, or $W = 0.89$ if a shorter value of $\Lambda_e = 4.0$ Å is used. These values thus suggest via $1 - W \approx 0.10$–0.11 only 3–4% more nondirect transitions at 295 K than the bulk values of $1 - W \approx 0.07$ would indicate.

3. *Data for ferromagnetic metals*

Finally, we consider the possible importance of phonon-assisted nondirect transitions on temperature-dependent photoemission from $3d$ ferromagnets.[15–18] In order to theoretically model such effects, we have performed cylindrically-broadened calculations for normal emission from Ni(001) at various photon energies between 43 and 103 eV so as to allow sampling of states along Γ–Δ–X, exactly as we have presented for Cu(001). We have used as $E^i, \mathbf{k}^i$ input values the self-consistent exchange-split band structure of Wang and Callaway[45] based on the von Barth–Hedin potential. The Fermi energy has been adjusted to place the highest $X_2(\downarrow)$ minority band at approximately 0.2 eV below E_F; this was done in order to yield an $X_2(\uparrow)/X_2(\downarrow)$ intensity ratio of approximately unity, as observed in spin-polarized photoemission by Hopster *et al.*[16] at a lower energy of $h\nu = 16.8$ eV. The theoretical exchange splittings are 0.55 eV for Γ_{12}, 0.54 eV for Γ'_{25}, and 0.57 eV for X_2, and these values are held constant as the degree of broadening is increased. Although no experimental data is yet available that can be directly compared to these calculations, we have chosen theoretical parameters to represent measurements at reasonably high angular and energy resolutions. An assumed angular resolution of $\pm 1.0°$ yields a $\Delta k^f_{\perp,\min}$ of $0.05(2\pi/a)$; $\Lambda_e = 5$ Å yields via $1/2\Lambda_e$ a $\Delta k^f_{\parallel,\min}$ of $0.06(2\pi/a)$ that is, for example, comparable to that needed in Fig. 13 for Cu(110); and a final Gaussian broadening with 0.1 eV FWHM simulates the energy resolution. As with the Cu(001) calculations, the isotropic broadening is increased in steps of $0.1(2\pi/a)$ in both $\Delta k^f_{\perp}$ and $\Delta k^f_{\parallel}$. Presented in Figs. 14 and 15 are the results of such calculations with various degrees of BZ averaging for $h\nu = 43.0$ eV, which corresponds to DT emission centered on the Γ point, and for $h\nu = 102.5$ eV, which corresponds to X-point emission.

The theoretical curves in Fig. 14 show very good resolution of the Γ'_{25} and Γ_{12} exchange splittings with minimum broadening [Fig. 14(f)], but by 6.5% broadening in Fig. 14(c), there is significant overlap of adjacent features and a concomitant decrease of the degree of spin polarization expected in most of the features. The Γ_{12} splitting as measured in a total intensity spectrum is also not clearly resolved with broadenings $> 6.5\%$, so that such effects could be falsely attributed to a reduction in the exchange splitting even though our calculations have held it constant. By contrast, the Γ'_{25} splitting is seen to persist as well-resolved peaks with a significant degree of spin polarization up to the highest broadenings considered here. This suggests that the Γ'_{25} doublet may be a preferred point of measurement to minimize spurious effects due to phonon-assisted NDT's. Prior analyses of photoemission data yield a range of Γ_{12} splittings from 0.1–0.9 eV and of Γ'_{25} splittings from 0.4–1.2 eV.[14,46,47] If either of these values are in fact on the lower end of these ranges, phonon effects could be even more important than suggested by Fig. 14. The Γ_1 intensity at highest binding energy also is shown here, but it exhibits no exchange splitting.

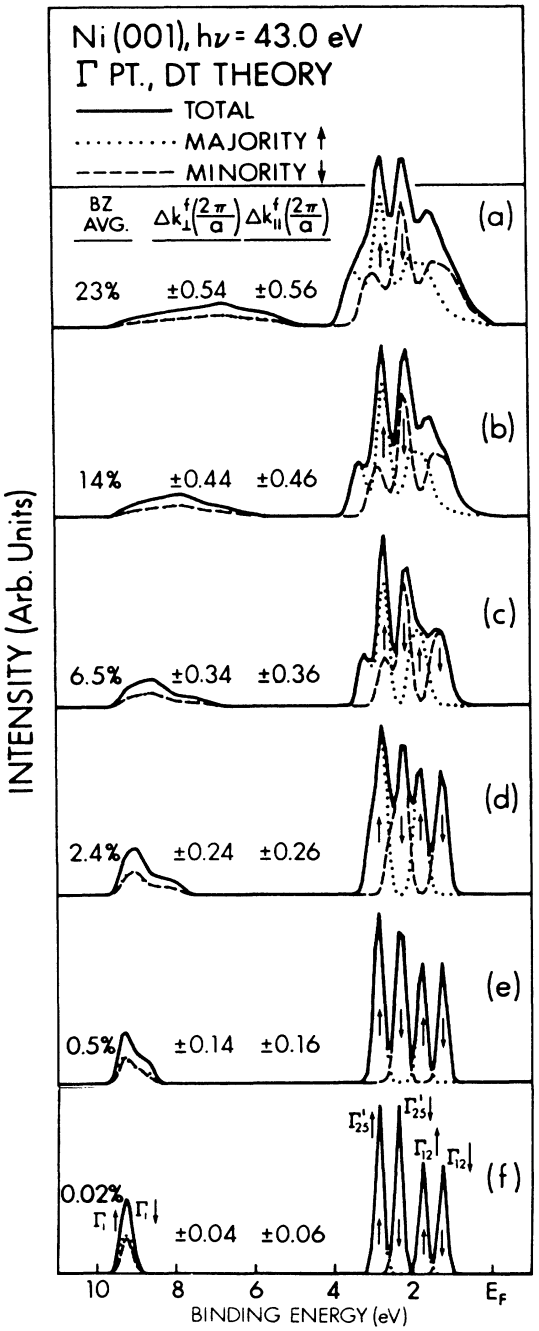

FIG. 14. Cylindrically-broadened direct-transition calculations simulating temperature effects for normal emission from Ni(001). The photon energy of 43 eV corresponds to direct transitions centered at the Γ point. The calculations are based on the band structure of Wang and Callaway (Ref. 45). Majority-spin intensity is indicated by dotted lines and minority spin by dashed lines.

The calculated curves in Fig. 15 exhibit good resolution of the X_2 splitting at minimum broadening [Fig. 15(f)], as well as outer peaks of unique spin makeup in the X_1-X_3 region. As the degree of zone averaging is increased, the degree of overlap between the two spin components again increases and the predicted total spectra exhibits a lowering of the ability to resolve these components. For example, the $X_2(\downarrow)$ peak broadens substantially to lower energies as **k** averaging is increased. By ~ 14—23% averaging, only this minority $X_2(\downarrow)$ feature nearest E_F is expected to exhibit a significant spin polarization, with the remainder of the spectrum having about equal contributions from both spins. If the exchange splitting were as small as 0.13 eV, a number consistent with certain experimental results,[16] the overlap and loss of both energy resolution and spin polarization in these features would be expected to be even greater.

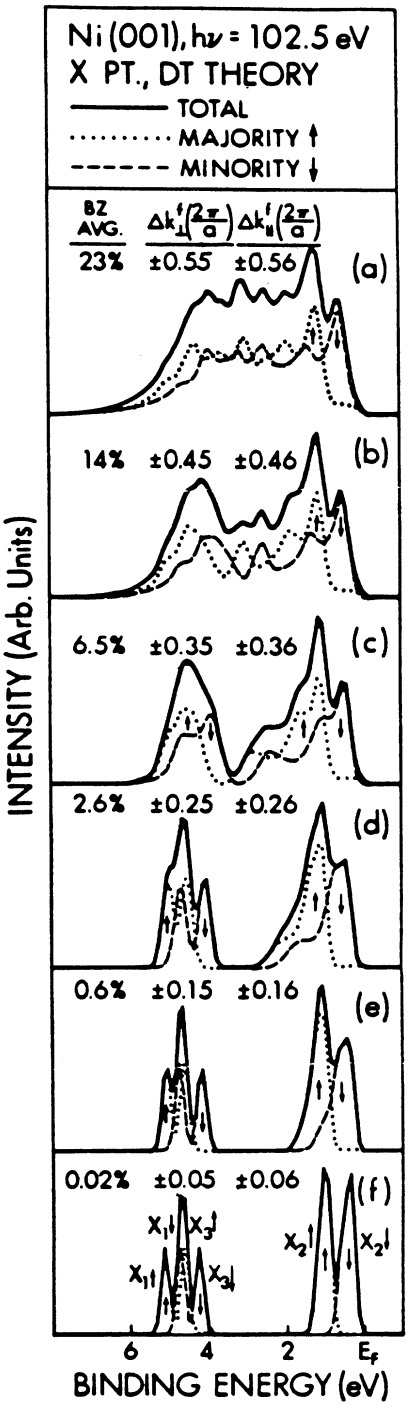

FIG. 15. As Fig. 14, except for $h\nu = 102.5$ eV corresponding to direct transitions centered at the X point.

In attempting to compare these calculations to possible experimental data for Ni, we can use the degrees of zone averaging empirically derived for Cu, and assume that the two metals will behave similarly as to phonon-assisted NDT's when both have the same value of the ratio T/Θ_D. For Ni, $\Theta_D = 450$ K and the Curie temperature $T_c = 627$ K. Thus, heating Ni to $> T_c$ to observe possible changes in the exchange splitting involves $T/\Theta_D > 1.39$. For Cu with $\Theta_D = 343$ K, this corresponds to a T of 477 K, and thus within the range of our experimental data. At this temperature, our data at various energies permit estimating a broadening of ~ 5—10% of the BZ due to NDT's. Thus, for this case, it seems certain that zone averaging due to nondirect transitions would not only significantly lower the degree of resolution of the two Γ_{12} peaks and the two X_2 peaks in standard photoemission spectra measuring total intensities, thus making it difficult to clearly distinguish a change in the exchange splitting with temperature, but also significantly reduce the degree of difference seen between spin-polarized photoemission spectra obtained at these two zone points. The experimental data of Hopster *et al.*[16] at lower $h\nu$, in fact, show the two X_2 peaks broadening and moving closer together. Although our estimates of NDT effects are based upon higher energies with an assumed $\mathbf{g} = (0,0,2)2\pi/a$, effective **g**'s of similar magnitudes are also expected at $h\nu = 10$—20 eV,[9–12,23] and it is thus significant that such additional zone averaging associated with phonons can produce effects on model spectra with a fixed exchange splitting that are very similar to those associated with a closing of the exchange splitting. Thus, phonon-assisted NDT's are potentially very important effects in such studies of ferromagnetic metals near T_c. As a rough indicator of the degree of importance, some T_c/Θ_D ratios and bulk Debye-Waller factors are, respectively, 1.39 and 0.91 for Ni, 2.22 and 0.79 for Fe, and 0.49 and 0.96 for Cr. Thus, for Ni and Fe very significant averaging over ~ 10—15% of the BZ is expected, with even larger effects possible if allowance is made for enhanced surface vibrational amplitudes. For Cr, effects of up to a few percent could be possible, and Figs. 12(c), 12(d), 14(d), and 15(d) indicate that even this could introduce significant spectral broadening that could be present in recent experimental data for this system.[17]

IV. CONCLUSIONS

Although a fully quantitative approach for including all aspects of the electron-phonon interaction in the photoemission process is still lacking, we have shown that the strong temperature effects observed in variable-energy

angle-resolved photoemission from Cu(001) and Cu(011) can be semiquantitatively explained in terms of phonon-assisted nondirect transitions (NDT's) that are preferentially located near the direct transition in **k** space. These effects are most critical in BZ regions with bands of high dispersion, where they can result in peak shifts on the order of 0.2—0.5 eV that agree well with Cu(001) experimental data for $h\nu=41-106$ eV. Such phonon-assisted NDT's are also clearly present at ambient temperature for Cu, and to a degree also even at 77 K. Thus, accurate band mapping via angle-resolved photoemission will require low-temperature measurements for many systems, and certainly for those with low Θ_D.

It is also clear that a rigorous decomposition of temperature-dependent data into direct and nondirect components cannot be carried out in a simple way, even if effectively lower Debye-Waller factors are used due to enhanced surface vibrations. We have discussed a more accurate model for phonon-induced NDT's including correlated lattice vibrations, and have suggested that it can be crudely approximated by a cylindrical broadening of simple direct-transition calculations in **k** space. This cylindrical broadening is used to simulate the expected peaking of phonon-assisted transitions about the direct-transition point. This type of broadening results in a semiquantitative description of temperature-dependent spectra for Cu(001) and Cu(011),[3] with estimated degrees of zone averaging largely due to NDT's of $\sim 1-3\%$ at 77 K, $\sim 3-9\%$ at 295 K, $\sim 9-20\%$ at 793 K, and $\sim 20-30\%$ at 973 K. It is not necessary to invoke a one-dimensional density-of-states model in order to describe this temperature-dependent data from Cu(001) and Cu(011), although the cylindrical broadening we have used includes certain features of this model as a limiting case.

Similar model calculations with cylindrical broadening for exchange-split Ni bands suggest considerable caution in interpreting the temperature dependence of these splittings in ferromagnetic materials.

ACKNOWLEDGMENTS

We are grateful to P. K. Lam and B. Sinković for helpful comments.

*Present address: IBM T. J. Watson Research Center, Yortown Heights, NY 10598.

†Present address: National Synchrotron Light Source, Brookhaven National Laboratory, Upon, NY 11973.

[1]E. W. Plummer and W. Eberhardt, in *Advances in Chemical Physics,* edited by L. Prigogine and S. A. Rice (Wiley, New York, 1982), Vol. XLIX; *Photoemission in Solids,* edited by M. Cardona and L. Ley (Springer-Verlag, Berlin, 1978), Vols. 1 and 2.

[2](a) N. J. Shevchik, J. Phys. C **10**, L555 (1977); (b) Phys. Rev. B **16**, 3428 (1977); (c) **20**, 3020 (1979).

[3]R. S. Williams, P. S. Wehner, J. Stöhr, and D. A. Shirley, Phys. Rev. Lett. **39**, 302 (1977).

[4]M. J. Sayers and F. R. McFeely, Phys. Rev. B **17**, 3867 (1978).

[5](a) J. A. Knapp, F. J. Himpsel, A. R. Williams, and D. E. Eastman, Phys. Rev. B **19**, 2844 (1979); (b) N. E. Christensen, *ibid.* **20**, 3205 (1979).

[6]Z. Hussain, S. Kono, R. E. Connelly, and C. S. Fadley, Phys. Rev. Lett. **44**, 895 (1980); Z. Hussain, C. S. Fadley, S. Kono, and L. F. Wagner, Phys. Rev. B **22**, 3750 (1980).

[7]S. D. Kevan and D. A. Shirley, Phys. Rev. B **22**, 542 (1980).

[8](a) C. G. Larsson and J. B. Pendry, J. Phys. C **14**, 3089 (1981); (b) J. B. Pendry, *Low Energy Electron Diffraction* (Academic, London, 1974), Chap. 6.

[9]H. Mårtensson, P. O. Nilsson, and J. Kanski, Appl. Surf. Sci. **11/12**, 652 (1982).

[10]H. Mårtensson, Phys. Rev. B **27**, 4492 (1983).

[11]H. Mårtensson, C. G. Larsson, and P.-O. Nilsson, Surf. Sci. **126**, 214 (1983).

[12]H. Mårtensson and P. O. Nilsson, Surf. Sci. **152/153**, 189 (1985).

[13]G. Jezequel, A. Barski, P. Steiner, F. Solal, P. Roubin, R. Pinchaux, and Y. Petroff, Phys. Rev. B **30**, 4833 (1984).

[14]D. E. Eastman, F. J. Himpsel, and J. A. Knapp, Phys. Rev. Lett. **40**, 1514 (1978); Phys. Rev. B **19**, 2919 (1979).

[15]C. J. Maetz, U. Gerhardt, E. Dietz, A. Ziegler, and R. J. Jellito, Phys. Rev. B **48**, 1686 (1982).

[16]H. Hopster, R. Raue, G. Güntherodt, E. Kisker, R. Clauberg, and M. Campagna, Phys. Rev. Lett. **29**, 829 (1983).

[17]L. E. Klebanoff, S. W. Robey, G. Liu, and D. A. Shirley, Phys. Rev. B **30**, 1048 (1984).

[18]E. Kisker, K. Schröder, W. Gudat, and M. Campagna, Phys. Rev. B **31**, 329 (1985).

[19]C. Caroli, D. Lederer-Rozenblatt, B. Roulet, and D. Saint James, Phys. Rev. B **8**, 4552 (1973).

[20]L. F. Wagner, Z. Hussain, C. S. Fadley, and R. J. Baird, Solid State Commun. **21**, 453 (1977); L.-G. Petersson, Z. Hussain, S. Kono, and C. S. Fadley, *ibid.* **34**, 549 (1980); Z. Hussain, S. Kono, L.-G. Petersson, C. S. Fadley, and L. F. Wagner, Phys. Rev. B **23**, 724 (1981).

[21]J. Stöhr, P. S. Wehner, R. S. Williams, G. Apai, and D. A. Shirley, Phys. Rev. B **17**, 587 (1978).

[22]T. C. Chiang, J. A. Knapp, M. Aono, and D. E. Eastman, Phys. Rev. B **21**, 3513 (1980).

[23](a) P. Thiry, D. Chandesris, J. Lecante, C. Guillot, R. Pinchaux, and Y. Petroff, Phys. Rev. Lett. **43**, 82 (1979); (b) P. Thiry, doctoral thesis, University of Paris, 1980.

[24]M. Sagurton (unpublished results).

[25]R. C. White, C. S. Fadley, M. Sagurton, and Z. Hussain, Phys. Rev. B **34**, 5226 (1986).

[26](a) B. E. Warren, *X-ray Diffraction* (Addison-Wesley, Reading, Mass., 1969), pp. 159—169; (b) R. W. James, *The Optical Principles of the Diffraction of X-rays* (Bell, London, 1954), pp. 193—228.

[27]J. T. McKinney, E. R. Jones, and M. B. Webb, Phys. Rev. **160**, 523 (1967).

[28]R. C. White, C. S. Fadley, M. Sagurton, P. Roubin, D. Chandesris, J. Lecante, C. Guillot, and Z. Hussain, Solid State Commun. **59**, 633 (1986).

[29](a) J. Hermanson, Solid State Commun. **22**, 9 (1977); (b) W. Eberhardt and E. W. Plummer, Phys. Rev. B **21**, 3245 (1980).

[30]G. A. Burdick, Phys. Rev. **129**, 138 (1963).

[31]M. Mehta and C. S. Fadley, Phys. Rev. Lett. **39**, 1569 (1977).

[32]G. D. Mahan, Phys. Rev. B **2**, 4334 (1973).

[33]P. J. Feibelman and D. E. Eastman, Phys. Rev. B **10**, 4932 (1974).

[34]C. S. Fadley, review in *Electron Spectroscopy, Theory, Techniques, and Applications,* edited by C. R. Brundle and A. D. Baker (Academic, London, 1978), Vol. II, pp. 59—65 and 136—142.

[35]G. Paasch, Phys. Status Solidi B **87**, 191 (1978).
[36]M. P. Seah, J. Phys. F **3**, 1538 (1973), and references therein; M. P. Seah and W. A. Dench, Surf. Interface Anal. **1**, 1 (1979).
[37]J. J. Barton and D. A. Shirley, Lawrence Berkeley Laboratory Report No. 14758, 1985 (unpublished).
[38]R. Couths, V. Bachelier, B. Cord, and S. Hüfner, Solid State Commun. **40**, 1059 (1981).
[39]J. F. Janak, A. R. Williams, and V. L. Moruzzi, Phys. Rev. B **11**, 1522 (1975); O. Jepson, D. Glotzel, and A. R. Mackintosh, *ibid.* **23**, 2684 (1981), and references therein.
[40]T. Grandke, M. Cardona, and L. Ley, Solid State Commun. **32**, 353 (1979).
[41]L. F. Ley, J. Electron Spectrosc. Relat. Phenom. **15**, 329 (1979).
[42]S. M. Goldberg, C. S. Fadley, and S. Kono, J. Electron Spectrosc. Relat. Phenom. **21**, 285 (1981).
[43](a) B. E. Hayden, K. C. Prince, P. J. Davies, G. Paslucci, and A. M. Bradshaw, Solid State Commun. **48**, 325 (1983); (b) G. Paslucci, K. C. Prince, B. E. Hayden, P. J. Davies, and A. M. Bradshaw, *ibid.* **52**, 937 (1984).
[44]R. S. Williams (private communication).
[45]C. S. Wang and J. Callaway, Phys. Rev. B **15**, 298 (1977).
[46]D. E. Eastman, J. F. Janak, A. R. Williams, R. V. Coleman, and G. Wendin, J. Appl. Phys. **50**, 7423 (1979).
[47]W. Eberhardt and E. W. Plummer, Phys. Rev. B **21**, 3245 (1980); F. Welling and J. Callaway, *ibid.* **26**, 710 (1982).